Journal of Materials Chemistry B

Accepted Manuscript

This article can be cited before page numbers have been issued, to do this please use: A. Rakovich and T. Rackovich, *J. Mater. Chem. B*, 2018, DOI: 10.1039/C8TB00153G.

ROYAL SOCIETY OF CHEMISTRY

rsc.li/materials-b

View Article Online
DOI: 10.1039/C8TB00153G

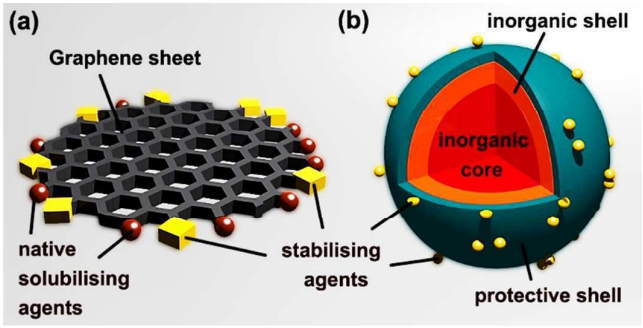

This review provides a comparison of optical, chemical and biocompatibility properties of graphene and semiconductor quantum dots as fluorescent probes.

View Article Online
DOI: 10.1039/C8TB00153G

Journal Name

ARTICLE TYPE

Cite this: DOI: 10.1039/xxxxxxxxxx

Semiconductor versus graphene quantum dots as fluorescent probes for cancer diagnosis and therapy applications

Aliaksandra Rakovich,*[a,b] and Tatsiana Rakovich[c]

Received Date
Accepted Date

DOI: 10.1039/xxxxxxxxxx

www.rsc.org/journalname

Early diagnosis of cancer is of critical importance in determining the outcome of a patient, and nanoparticulate fluorophores have been at the centre of research for such applications owing to their superior optical properties. Furthermore, the large surface area to volume ratios of these fluorophores enables them to be endowed with several modalities, including the targeting of specific biomarkers and drug delivery capabilities, promoting them as therapeutic agents as well. Over the last few decades, semiconductor quantum dots have dominated the field due to their unique yet well characterised optical properties. However, the scope of their application for diagnosis and therapy of cancer has been hindered by declarations of *in vivo* toxicity attributed to heavy metals typically found in their composition. Recent arrivals graphene quantum dots, or carbon-derived counterparts to SQDs, are often claimed to be biocompatible but they have complicated optical properties. In this review, we compare the properties of these two types of quantum dots in view of their employment as fluorescent agents for cancer diagnosis and therapy.

1 Introduction

A few years ago, the UK media made an announcement that the lifespan of over half of new cancer patients would be extended by a decade[1]; this means that the average 10-year survival rate in the UK would finally increase to 50%! Indeed, for the UK the overall trend across decades has been one of declining mortality rates[2] (Figure 1a, data in red), which is attributed to the great therapeutic advances and improvements in diagnostic methods, the latter also being largely responsible for detection of the rising amounts of cancer incidences in the last few decades (Figure 1a, data in blue). However, this view can be misleading, as can be evidenced by similar time trends for the four most occurring cancer types: lung, breast, bowel, and prostate. For example, the net survival rates for breast and prostate cancers have both increased to 80% by 2010, and so they weigh heavily in the statistics (blue and green bars in Figure 1b). On the other hand, the survival rate for lung cancer has remained below 5% (red bars in Figure 1b), despite the extraordinary advances in oncology mentioned above.

Great insight into this discrepancy can be gained by examining the stage of cancer development at which it is more likely to be diagnosed. Both breast and prostate cancer have a higher incidence of cancers diagnosed at stage I compared to lung cancers, which are most likely to be diagnosed at stage IV, i.e. when it has already metastasized throughout the body (Figure 1c). This, combined with higher survivability rates for earlier stages of cancer (Figure 1d), elucidates the criticality of early diagnosis - it is the single most important factor in determining the outcome for the patient.

Several factors can promote early diagnosis. Public awareness can be raised about the symptoms and the simple do-it-at-home self-checks, as has been the case for breast cancer. Also, the availability of simple screening methods based on detection of biomarkers in blood samples could be increased, as was the case for prostate cancer around 1990 when PSA testing was introduced (indicated by * in Figure 1b), correlating with the jump in the net survivability rates for prostate cancer from pre-1990 to post-2000 (Figure 1b). These, however, are special cases of easily accessible and commonly occurring cancers. The vast majority of cancer types do not fall within this category, and it is in these cases where major scientific advances are urgently needed.

Among various types of diagnostic detection methods, fluorescence-based techniques offer unique practicalities, such as high sensitivity, specificity, activatable signal and multiplexing capabilities, fast acquisition times, and the widespread availability and relatively low cost of instrumentation[3,4]. Such detection techniques rely on the use of a fluorophore, which traditionally has been a molecular dye. However, a vast amount of research in

[a] *Photonics and Nanotechnology Group, Department of Physics, King's College London, London, United Kingdom. Tel: 02 07848 7328; E-mail: aliaksandra.rakovic@kcl.ac.uk*
[b] *Experimental Solid State Group, Department of Physics, Imperial College London, London, United Kingdom.*
[c] *Department of Molecular Rheumatology, Trinity Biomedical Sciences Institute, Trinity College Dublin, Dublin 2, Ireland.*

View Article Online
DOI: 10.1039/C8TB00153G

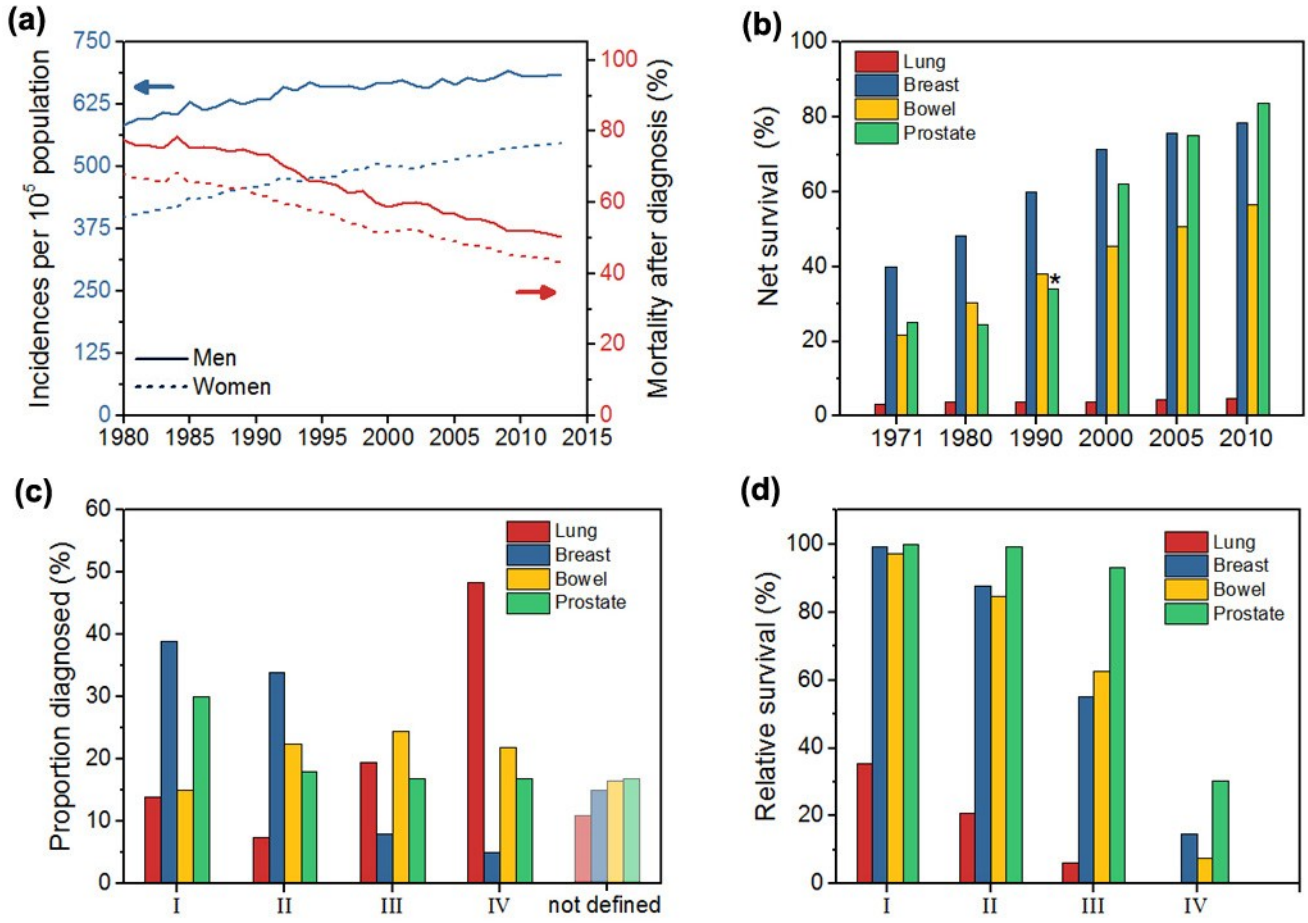

Fig. 1 Cancer incidences and mortality rates in the United Kingdom. Panel **(a)** shows incidences of diagnosis of cancer per 100,000 of population (blue lines) and subsequent mortality rate (red lines) for men (solid lines) and women (dashed lines) in UK from 1980 to 2015. Panel **(b)** shows the net 10-year survival percentage for four most commonly diagnosed cancer types from 1971 to 2010. The bottom panels show proportion of total diagnosis made **(c)** and the relative 5-year survival percentage **(d)** per stage of cancer progression. Data obtained from Cancer Research UK, http://www.cancerresearchuk.org/health-professional/cancer-statistics/, accessed January 2017.

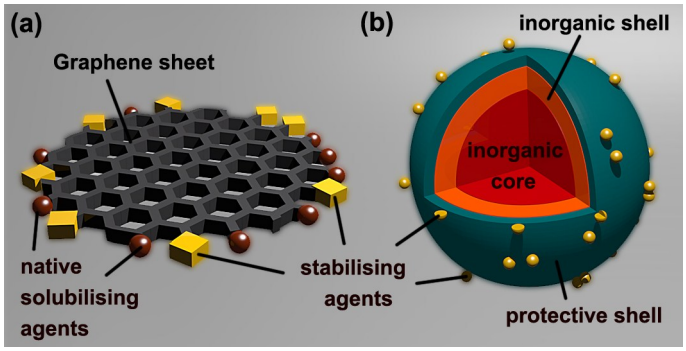

Fig. 2 Diagramatic representation of the structures of graphene (a) and semiconductor **(b)** quantum dots. The two types of quantum dots both have similar sizes (Table 1), and are stabilised by hydrophilic groups attached to their surfaces/edges (yellow squares/spheres). The core of the GQDs consist of a single or few layers of grapene sheets. SQDs have inorganic cores (red), sometimes surrounded by a shell of another inorganic material (orange). They may also be encapsulated in additional layer for stability purposes or to reduce the toxicity of heavy-metal containing SQDs.

the cancer detection field in the last few decades has been dominated by colloidal semiconductor Quantum Dots (SQDs). These are nanometre-sized crystals of semiconductor materials such as CdSe, ZnS, InP, and PbSe kept in solution through the attachment of stabilising ligands to their surfaces (Figure 2b). They have very appealing size-dependent optical properties, including symmetric emissions and high fluorescence quantum yields[4,5]. Their popularity over the years for *in vitro* bioimaging and immunosensing assays is a reflection of these properties[6,7], and thus many regard SQDs to be at the forefront of the race for the development of next-generation medical diagnostic tools. Likewise, the large surface area to volume ratios of SQDs presents an exciting opportunity for the attachment of multiple agents to their surfaces to yield combined diagnostic and therapeutic modalities. However, many consider SQDs unsuitable for *in vivo* applications due to reports of toxicity issues relating to the presence of heavy metals commonly found in their composition[8–10]. In addition, the availability of said elements in nature is relatively low and therefore SQDs are considered to be expensive. It should be noted that these claims are gross generalisations, especially in view of the

View Article Online
DOI: 10.1039/C8TB00153G

limited amount of comprehensive studies published on the topics. Nevertheless, they have somewhat obstructed the translation of SQDs to therapeutic and diagnostic applications.

Carbon, on the other hand, is abundant, inexpensive and is generally considered to be biocompatible. Although the link between material composition and its biocompatibility is not straightforward, graphene Quantum Dots (GQDs) – or carbon equivalents to SQDs – have emerged as potential alternatives. GQDs are generally described as a single- to few-layer patches of graphene sheets, with lateral dimensions in the nanometre range[11] (Figure 2a). They offer many exciting opportunities for drug delivery and photodynamic therapy, as will be discussed in later sections, but do have complicated fluorescence behaviour[12–16]. Despite this fact, and an almost complete lack of information about their *in vivo* toxicity, they have already established themselves as significant contenders in the field.

In this review, we compare the properties of two types of quantum dots in the context of using them as fluorescent labels for diagnosis and therapy of cancer. As a reference, we use the guiding principles of Resch-Genger *et al.*[4] for a suitable label, which include: (1) the optical properties of the probes, such as their brightness, photostability and convenient excitation; (2) their chemical properties such as the solubility, stability under experimental or physiological conditions, availability of chemical modification strategies for labelling and drug loading; (3) the potential toxicity and biocompatibility of the label. We should note that the aim of this review is not to deliver an extensive summary of the literature, but rather to provide a critical comparison of the two quantum dots types in order to facilitate the choice between them for a particular application. There exist a great number of reviews for both types of quantum dots, and where possible, the reader is directed to them for more detailed accounts of specific topics.

2 Comparison of optical properties

The optical properties relevant to the application of quantum dots as fluorescence probes include their linear optical properties, such as the wavelength and quantum yield of their emission, and their absorption properties in the visible and the biologically-significant spectroscopic ranges, and their photostability. Other properties that may be significant for some applications are the shape of their photoluminescence bands, emission anisotropy (polarisation dependence), the fluorescence lifetime, and the non-linear absorption properties.

2.1 Origin of photoluminescence

When a semiconductor material absorbs a photon, an electron is promoted from the valence band to the conduction band, leaving behind a hole. Being of opposite charges, the electron-hole pair weakly binds to form a hydrogen-like quasi-particle called exciton, that has a corresponding binding radius called the exciton Bohr radius. In SQDs, the size of the particle is smaller than the Bohr radius, resulting in quantum confinement of the exciton and quantisation of its energies, the latter being inversely proportional to the size of the quantum dot[17–20]. Optical excitations be-

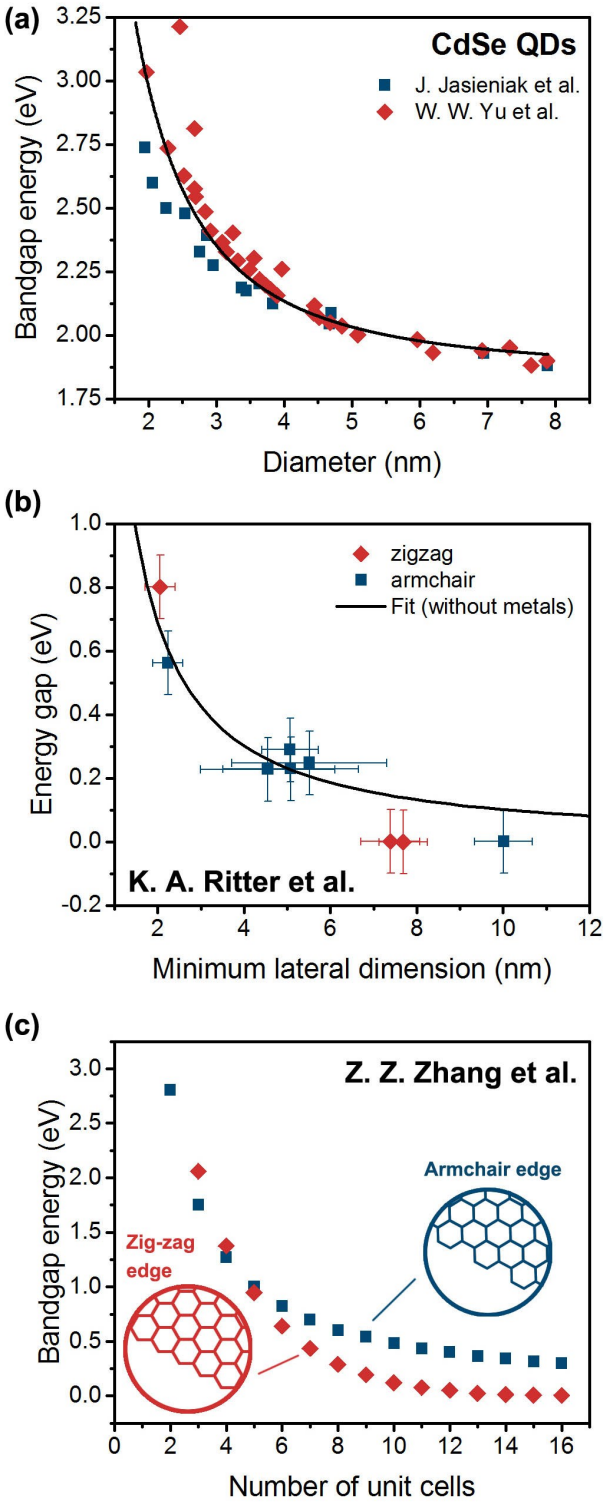

Fig. 3 Size-dependent optical properties. (a) The energy bandgap of SQDs as a function of their size is illustrated using data for CdSe quantum dots from two references[17,18]. Both sets of data do not significantly deviate from the expected $1/d^2$ dependency (black line). **(b)** and **(c)** illustrate the effect the edge geometry has on the bandgap of graphene-derived materials. (b) was obtained using electrical measurements on graphene nanoribbons and (c) are theoretical calculations for hexagonal GQDs. (b) was adapted from K.A. Ritter *et al.*[12]. (c) was adapted from Z. Z. Zhang *et al.*[16]

View Article Online
DOI: 10.1039/C8TB00153G

tween these discreet states give rise to the distinctive absorption spectra of SQDs, and band-edge recombination from the lowest excited state yields the characteristically narrow and symmetric emissions. It is important to point out that, for SQDs, the probability density for the excited electron is largest inside the confining potential and very small at its edge[21,22], i.e. at the surface of the quantum dot. Hence, for a well-confined SQD, its main optical properties, such as the emission wavelength and absorption spectrum, are defined primarily by its bulk, i.e. by the constituent material, its crystallinity, size, and shape. The photoluminescence quantum yield (PLQY) of the SQDs can be affected by changes to its surface, for example, through the creation of surface defects leading to the existence of non-radiative trap states[23–25]. Nevertheless, further chemical modification of well-passivated SQDs does not modify their optical properties significantly[4,26], typically resulting in a slight decrease of their PLQY and sometimes in a slight shift of their photoluminescence band (usually of the order of 10 nm).

Graphene is a zero-bandgap semiconductor, and the lack of the bandgap prohibits fluorescence in extended graphene structures. However, graphene can be made fluorescent by opening up a bandgap, which can be achieved in several ways, e.g. through the introduction of structural defects, the creation of small "sp2 islands" or the reduction graphene sheet size[27–30], as is the case for GQDs. In general, fluorescence in graphene-derived nanomaterials is attributed to two origins[15]: (a) transitions between states associated with the conjugated π-domains (islands of sp2 hybridisation character), similar to those found in large aromatic molecules; (b) defect-derived fluorescence, where the defect can either be electronically coupled to or act as a perturbation centre of the aromatic network.

The bandgap transitions in origin (a) are highly sensitive to their environment — any disturbance of the conjugated domains leads to a decreased efficiency of bandgap fluorescence; for example, the addition of the second layer of graphene strongly quenches said transitions[28]. Furthermore, even for pristine single-layer GQDs, the size-fluorescence relationship is more complex than for the case of SQDs due to the "quasi-molecular" nature of the fluorescence[14,31]. For example, nano-sized graphene pieces of similar sizes can have different bandgap energies depending on which type of edge is predominant in the structure (Figure 3)[12,16]. Moreover, and in contrast to SQDs, the ground states of the conduction and valence bands of nano-sized graphene have a non-zero value at their edges[16]. Therefore, any chemical modification of the edge groups, e.g. for solubility or functionalisation purposes, has the potential to affect the optical properties of GQDs. In practical terms, this means that, when designing fluorescence GQD probes, any post-synthesis chemical modifications must be taken into account. On the other hand, this effect has been exploited to enhance the fluorescence of GQDs by doping or edge functionalisation - the addition of strong electron donating or accepting moieties can strongly disturb the local electronic environment and modify the optical behaviour of GQDs[32–34]. Such defect-derived fluorescence tends to be much stronger than the bandgap transitions discussed above; in fact, it has been suggested that most of the strongly fluorescent GQDs have this type of emission[15]. In fact, one can argue that in most of the reports on fluorescent GQDs, this is the dominant type of photoluminescence mechanism, since no clear correlation exists between the lateral size of the colloidal GQDs and the energy of their emission (see Figure 4a).

2.2 Quantum dot brightness

The brightness of a fluorophore is defined as the product of its excitation cross-section (or extinction coefficient) at the excitation wavelength and its quantum yield. Effectively, it is a measure of the fluorescence signal that can be obtained with the given fluorophore and, along with some other parameters such as the width of emission, it has an influence on the resolution and contrast that can be obtained in bioimaging applications. A key point to take away from this is that the use of the fluorophore for bioimaging is determined by both its absorption and emission properties, and factors that influence both must be taken into account. It is therefore very unfortunate that in the majority of reports on the use of GQDs for these purposes, the authors fail to state the absorption coefficient of the sample. In fact, in our literature search for this review, we have come across only two that state this value: L. Wang *et al.*[33] reported a value of $\sim 10^6$ M^{-1} cm^{-1} at $\sim$400 nm excitation for GQDs emitting at 480 nm with a 45% Quantum Yield, while X. Yan *et al.*[35] reported a value of 10^5 M^{-1} cm^{-1} at the lowest energy peak (600 nm) and at 400 nm but did not report the emission characteristics of the sample. Ignoring the discrepancy of the order of magnitude between the two extinction coefficients quoted, these values are similar or lower to those reported for SQDs in similar wavelength ranges.

For example, as a measure of like-to-like comparison, the extinction coefficient of CdS SQDs emitting at 480 nm ($\sim$5.3 nm in size) is just under 10^6 M^{-1} cm^{-1} at 400 nm (according to W. W. Yu *et al.*[18]). Aqueous CdS SQDs with near unity quantum yields have been previously synthesised[36], making SQDs in this report slightly brighter than GQDs synthesised by L. Wang *et al.*[33].

The data in Figure 4 suggests that quite a significant portion of GQDs synthesised emit in the 500-600 nm region, hence it would be interesting to compare the brightness of these GQDs to SQDs. However, no extinction data is available for this wavelength range for GQDs, and so only estimates can be made. Based on the extinction values quoted above and data in Figure 4 for GQDs, the extinctions of SQDs and GQDs in the 500-600 nm spectral region are expected to be comparable, while the PLQY to be slightly higher for SQDs. On average, the expectation is that the two types of Quantum Dots would have similar brightness in this wavelength range.

For visible wavelengths above 600 nm, the extinction coefficients of SQDs are higher than those reported by X. Yan *et al.*[35] for GQDs: CdSe/ZnS SQDs with a first excitonic peak at 600 nm have an extinction coefficient of the order of 10^6 M^{-1} cm^{-1} and 2-3 times larger at 400 nm[18]. Furthermore, CdSe-based SQDs have consistently high PLQYs in this wavelength region (typically > 50%)[37–40] but have also been synthesised with near-unity PLQYs[41]. In contrast, very few GQDs have been synthesised with emissions above 600 nm (Figure 4a), and none of those report

View Article Online
DOI: 10.1039/C8TB00153G

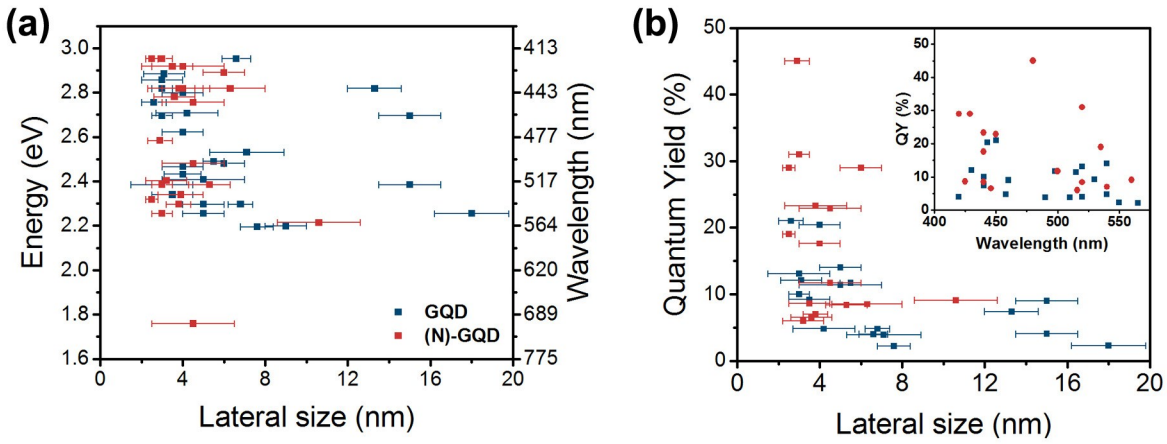

Fig. 4 Optical properties of synthesised graphene quantum dots. (a) Energy (scale on the left) and wavelength (scale on the right) of photoluminescence and **(b)** photoluminescence quantum yield as a function of lateral size of synthesised GQDs. Inset of (b) compares the quantum yield and wavelength of emission of GQD samples — no correlation between these parameters can be seen. Data points in blue are for non-doped GQDs with oxygenated end groups, those shown in red are for nitrogen-doped GQDs or GQDs with N-containing end groups. Data for both plots is summarised in Table 2.

their PLQY values. However, based on the data for typical GQDs (Figure 4b), their PLQY values in this region are expected to be below 50%. Therefore, the brightness of SQDs is expected to be almost an order of magnitude larger in this wavelength region.

Finally, the near-infrared (NIR) spectral region is of particular importance for bioimaging *in vivo*, since absorption by physiological fluids is minimal in this region allowing for deeper tissue visualisation[42]. The SQDs and GQDs have been proposed as suitable probes for these applications, although the literature for both is rather limited making the comparison between the two impractical.

For GQDs, M. Nurunnabi *et al.*[43] reported on the synthesis of NIR GQDs from carbon fibre, in which the temperature of the reaction could be used to control the wavelength of the emission: for temperatures below 80°C GQDs emitting in the NIR were produced. Neither the extinction coefficient nor the PLQY of the GQDs was stated in this case. L. Tang *et al.*[44] synthesised heavily N-doped GQDs which had three distinct photoluminescence peaks, including one in the NIR region which shifted depending on the size of the particle. In this case, the authors do quote the PLQY of ~11.3%, however, this value is for the emission in the visible and not in the NIR region.

For SQDs, S. Kim *et al.*[45] used type II CdTe/CdSe SQDs for sentinel lymph node mapping during a surgical procedure on small and large animals. The quantum yield of these QDs was 13%, and their extinction coefficient at first excitonic peak was ~$6x10^5$ M^{-1} cm^{-1}. W. Cai *et al.*[46] employed very large CdTe SQDs for *in vivo* imaging of integrin $\alpha_V\beta_3$-positive tumor vasculator in a murine xenograft model. Neither PLQY nor an extinction coefficient are stated, but the latter can be estimated to be ~$5x10^5$ M^{-1} cm^{-1} (according to W. W. Yu *et al.*[18]). J. P. Zimmer *et al.*[47] developed a method to synthesise core-shell InAs/ZnSe SQDs of various sizes that emit in the NIR, and then utilised these SQDs for sentinel lymph node mapping and extravasation from the vasculature in rat models. The synthesised SQDs had relatively low PLQYs of 6-9% after solubilisation in aqueous solution. The extinction coefficient of these SQDs is not mentioned in the paper, but typical values for InAs SQDs are of the order of 10^5 M^{-1} cm^{-1} at these wavelengths[48]. More recently, J. Park *et al.*[49] developed water-soluble NIR SQDs that did not have toxic elements in their composition and showed their applicability for *in vivo* biomedical imaging using a mouse model. These SQDs had relatively high extinction coefficients of ~$3x10^6$ M^{-1} cm^{-1} and good PLQYs of 20-30%, making them one of the best NIR probes to date.

2.3 Nonlinear optical properties

Multiphoton microscopy (MPM) is another type of imaging that makes use of increased transparency in the NIR region. One can think of it as a reverse of NIR imaging — the fluorophore is excited in the NIR but emits in the visible spectrum. Such upconversion, i.e. an increase in the energy of the emission relative to the excitation energy, can be due to multiple absorptions of low-energy photons involving virtual levels or defect-states, and these optical processes have nonlinear dependencies on the intensity of the excitation laser ($\propto I^2$ for two-photon absorption) leading to improved resolution of the technique compared to NIR imaging. Other advantages of MPM include higher quantum efficiencies and reduced photobleaching of fluorescent probes, reduced photodamage of biological tissues and minimised autofluorescence backgrounds[50,51]. The suitability of the fluorescent probe for MPM applications is often judged based on its multi-photon absorption cross-section (σ); for two-photon processes this is generally expressed in units of Göeppert-Mayer (GM).

Based on the tunability of their emission, high two-photon absorption cross-sections and very high quantum yields in the visible, SQDs have long been considered for these applications[52,54–65]. However, only a few examples exist of their application in cancer research and even fewer reference the nonlinear absorption cross-sections of SQD samples used. For example, D.R. Larson *et al.*[52] used MPM to image CdSe SQDs hundreds of mi-

View Article Online
DOI: 10.1039/C8TB00153G

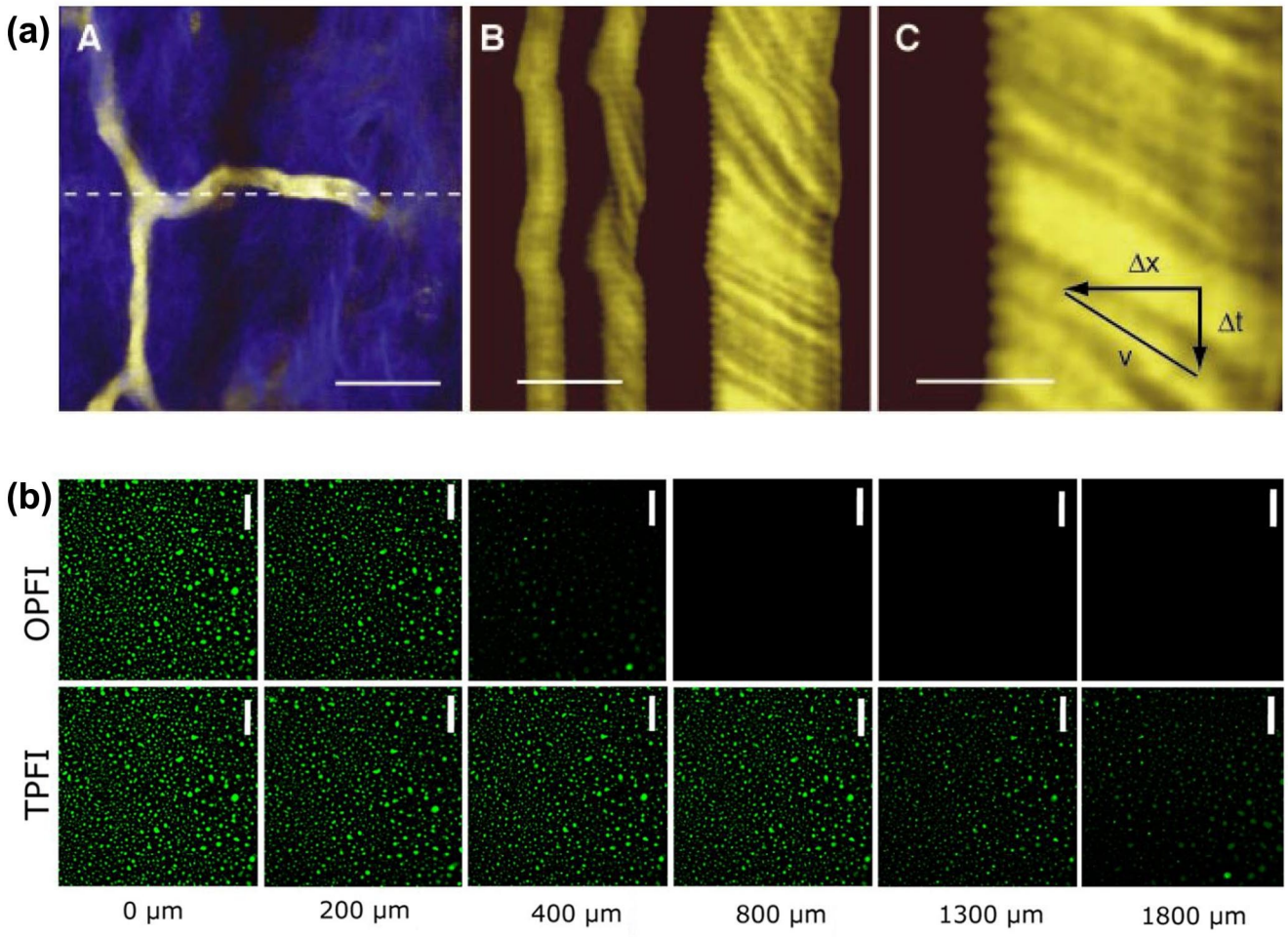

Fig. 5 Quantum dots as fluorescent probes for multi-photon microscopy. (a) Two-photon fluorescence microscopy of living mice tissues using CdSe SQDs with yellow emission, showing (A) capillaries at the base of the dermis, (B) a series of line-scan measurements across the region indicated in A, from which blood flow velocity was calculated, and (C) zoom section of B where undulations of capillary walls due to heartbeat are clearly visible. The blue background in (A) is due to second harmonic generation by collagen at 450 nm. Adapted from D.R. Larson *et al.*[52]. Reprinted with permission from AAAS. **(b)** One-photon (top row) and Two- photon (bottom row) fluorescence imaging (OPFI and TPFI respectively) of intralipid mock tissues at different depths, increasing left-to-right, using N-GQDs as probes. Adapted with permission from Q. Liu *et al.*[53]. Copyright (2017) American Chemical Society.

crometres below the skin of living mice and were able to visualise capillaries, measure blood flow and estimated the heart rate of mice from undulations of the capillary walls (Figure 5a). They reported action cross-sections (product of σ and PLQY) of up to 47,000 GM for these QDs, depending on the excitation wavelength. Since the PLQYs are less than 1.0, the actual values of σ are expected to be even higher, i.e. close to the theoretical value for CdSe QDs of 50,000 GM[66]. More recently, H. Hafian *et al.*[61] have employed CdSe/ZnS SQDs conjugated with single-domain antibodies for two-photon imaging of carcinoembryonic antigen in human appendix and colon carcinoma tissue sections. While the depth of the imaging, in this case, was relatively low, the study does demonstrate the pertinence of this technique to discrimination of normal and cancerous tissues. The probes used in this study had σ of up to 49,000 GM.

As far as GQDs are concerned, a number of reports have been published demonstrating upconversion in GQDs[34,69–71], but only two report their use for MPM imaging. In 2013, Q. Liu *et al.*[53] reported very high two-photon absorption cross-sections of 48,000 GM for N-doped GQDs excited at 780 nm, which they then utilised for MPM of HeLa cells at relatively low incident power. Furthermore, using intralipid mock tissue, they estimated the maximum penetration depth of the technique with their probes to be as large as 1800 μm (Figure 5b). In 2016, W.-S. Kuo[72] *et al.* developed an integrated method based on two-photon excitation of GQDs to simultaneously localise bacteria at a specific depth in a three-dimensional environment and eliminate the targeted bacteria using the photo-induced production of reactive oxygen species. The authors report a comparable value for two-photon absorption cross-section for their GQDs of 47,903 GM. Taking into account the random orientation of GQDs in these samples, both values are still about an order of magnitude lower than the theoretical estimates ($>10^6$ GM)[73] leaving a lot of room for improvement. Therefore, GQDs have great potential to become the preferred option for applications in MPM. However, as things stand at the moment, their nonlinear cross-sections are similar to those

View Article Online
DOI: 10.1039/C8TB00153G

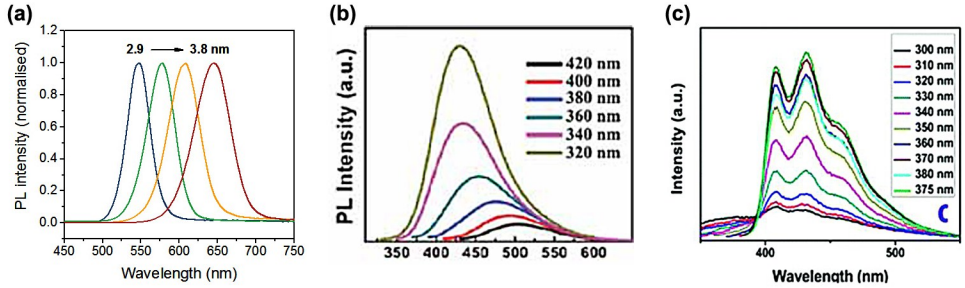

Fig. 6 Shape of photoluminescence bands of semiconductor (a) and graphene **(b,c)** quantum dots. **(a)** The symmetric photoluminescence profiles of four CdTe quantum dot samples of increasing diameters (the range of average diameters is indicated on the figure). **(b)** An example of a symmetric emission from GQDs. Reprinted from D. Pan *et al.*[67] with permission. **(c)** An example of asymmetric emission: the triple-picked photoluminescence profile of N, F and S co-doped quantum dots reported by S. Kundu[68]. Reprinted with permission. GQDs in (b) show a shift in photoluminescence position depending on excitation wavelength, while in those in (c) only vary in intensity (excitation wavelengths for both are shown in the legend).

of SQDs while their PLQYs are slightly lower (see above section), making their two-photon action cross-sections slightly lower too.

2.4 Shape of photoluminescence bands

While the shape of the PL band of the fluorescent label may be of reduced importance in bioimaging, it gains prominence in applications involving multiplexed detection, which rely on the deconvolution of contributions from individual channels. In this respect, SQDs have gained immense reputation due to their symmetric emission profiles (Figure 6a), originating from the characteristic band-edge emissions, broadened by the Gaussian distribution of their sizes in a typical colloidal sample. Recently, D. Ren *et al.* used two SQD samples simultaneously, one labeled with epidermal growth factor (EGF) and the other with the antibody against the epidermal growth factor receptor (EGFR). This was done in order to study what role EGFR plays in preventing HeLa cells from engulfing EGF and in inhibiting the overproliferation of the cells[74]. Q. Xu *et al.* used triplexed Förster Resonance Energy Transfer (FRET)-based detection to develop a chemical 'nose' for differentiation of serum proteins and cell lines. Their multiplexed sensing platform was able to correctly distinguish between ten different serum proteins, seven proteins in human serum and identify seven human cell lines, six of which were cancerous, all without the need for a spatial array separation and at single excitation wavelength[75]. Similarly, X. Qiu and N. Hilderbrandt used a time-gated FRET between a Tb complex and three appropriately-labeled SQDs to simultaneously detect three corresponding microRNA biomarkers. The triplexed detection assay required no washing or separation steps and achieved a sensitivity of $\sim$0.2 nM[76]. For earlier examples and further details on the use of SQDs for multiplexed applications, readers are directed to the reviews from E. Petryayeva *et al.*[77] and G. Rousserie *at al.*[78]; in addition, the book chapter by N. Hildebrandt and D. Geißler in "Nano-Biotechnology for Biomedical and Diagnostic Research" includes FRET-based multiplexed diagnostic applications of SQDs[79].

In contrast to SQDs, the vast majority of GQDs are reported to have asymmetric emission profiles (Table 2), originating from the "quasi-molecular" electronic structure of GQDs discussed above. Furthermore, chemical functionalisation of edges or doping of GQDs, e.g. to enhance their PLQY, can add to the complexity of the PL shape. For example, S. Kundu *et al.* synthesised N, F and S co-doped GQDs that had a triple-peaked emission (Figure 6c)[68]. However, some examples of symmetric photoluminescence bands of GQDs have been reported in the literature (Figure 6b and Table 2). Regarding colour-multiplexed applications of GQDs, the situation is further complicated by the excitation wavelength-dependent emission often observed with GQDs. The proposed origin of this effect is an optical selection of different electronic states associated with various surface defects of GQDs and/or selection of differently-sized GQDs as the excitation wavelength is scanned[80–82]. The difficulty in accounting for these photoluminescence characteristics, and their variability across different samples, makes multiplexed application of GQDs difficult, and this has been reflected by a lack of work in this area. Perhaps the only application of GQDs for multiplexed detection relating to cancer diagnosis to date has been that reported by Z. S. Qian *et al.* who developed a dual-sensor platform for simultaneous detection of DNA and bovine α-thrombin. In this work, two GQDs were bonded with a specific oligonucleotide sequence and a thrombin aptamer respectively and then stacked on top of a graphene oxide sheet to provide the multiplexed "on-off-on" type detection platform[83].

2.5 Fluorescence lifetimes

Fluorescence lifetime is broadly defined as the average time a fluorophore spends in an excited state, or equivalently, the time for the excited state population to decay to 1/e via all possible radiative and non-radiative channels[109]. An interesting feature of the fluorescence lifetime is that it is much more sensitive to the local physicochemical environment of the fluorophore compared to its other optical properties[4,110]. Hence, parameters such as the local pH and temperature, the presence of ions and metabolites, and any interactions between the fluorophore and proteins, membranes, photosensitisers, etc. can all be visualised[110–112], providing a sensitive measure of the intra-cellular environment. Furthermore, fluorophores of different types tend to have widely different fluorescence lifetimes; hence, concurrent intensity and lifetime measurements can be used to easily deconvolve (or un-

View Article Online
DOI: 10.1039/C8TB00153G

Table 1 Comparison of optical properties of semiconductor and graphene quantum dots

Property	Semiconductor QDs	Graphene QDs
Range of emission	Tunable from 400 to 1400 nm	Typically 400-600 nm[a]
Shape of emission spectrum	Symmetric emission bands with Gaussian profiles (size dispersion related)	Generally asymmetric, "quasi-molecular"
FWHM of emission spectrum	20-50 nm in the visible 50-100 nm in the NIR	FWHM typically <100 nm
Excitation dependence	Emission position does not vary significantly	Excitation-wavelength dependent emission likely
Polarisation dependence	No inherent dipole - all polarisations equivalet	Some polarisation dependency (in and out of plane of graphene sheets)
De-excitation behaviour[b]	Typically multi-exponential[c] Average lifetimes 10-100 ns	Typically multi-exponential Average lifetimes 1-10 ns
Quantum Yield	Visible: typically 40-70%; up to 95% NIR: typically 20-40%; up to 80%	Visible: typically 5-25%; up to 45% NIR: no data
Molar extinction coefficient	10^5-10^6 M^{-1} cm^{-1} at first excitonic peak	10^5-10^6 M^{-1} cm^{-1} at first excitonic peak
Two-photon cross-section	Up to 49,000 GM	Up to 48,000 GM
Stokes shift	Up to 100 nm	Typically 70-120 nm
Photostability	High; can observe photobrightening	High; can observe photobrightening

[a] Heavily doped GQDs have been shown to have fluorescence outside this range
[b] FLIM applications require contrast with autofluorescence, whose lifetime is typically of the order of 1-2 ns
[c] Behaviour can be monoexponential when surface of QDs is fully passivated

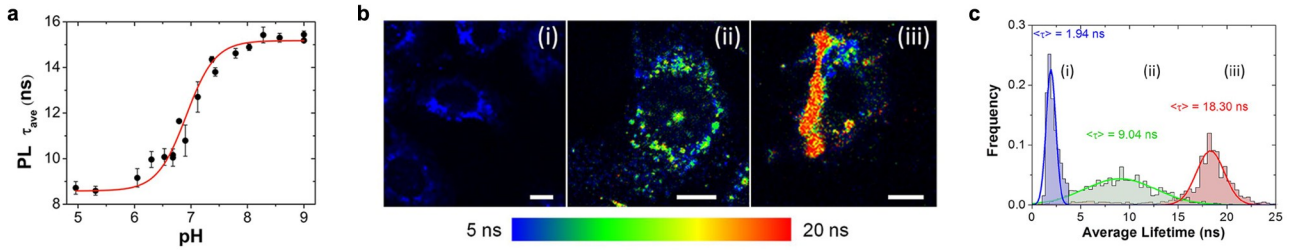

Fig. 7 Mercaptopropionic acid (MPA)-capped CdSe/ZnS quantum dots as intracellular pH sensors. (a) Fluorescence lifetime of MPA-SQDs as a function of pH of the synthetic intracellular buffer. FLIM image **(b)** and lifetime distribution **(c)** of MC3T3-E1 cells before (i) and after incubation with MPA-SQDs with nigericirin and buffers at pH 4.87 (ii) and 8.14 (iii). Reprinted with permission from A. Orte *et al.*[84] Copyright 2013 American Chemical Society.

mix) fluorescence images into contributions from different fluorophores even if they emit in the same spectral range, and/or to improve the contrast between different channels in multiplexed applications. This is of particular consequence in bioimaging, where autofluorescence can contribute strongly across a wide spectral range[113,114].

It is surprising, therefore, that these opportunities have remained largely unexplored for both types of quantum dots, despite the fact that their lifetimes are significantly larger than that of the autofluorescence (Table 1), and so both are well suited for fluorescence lifetime imaging microscopy (FLIM) studies involving cancerous cells. To date, no such investigations have been reported for GQDs and very limited literature exists for SQDs. The work by Grecco *et al.* was perhaps the earliest example of the application of SQDs to image a signal transduction process in live cells[115]. Specifically, they used CdSe/ZnS quantum dots to monitor clathrin-mediated transferrin-endocytosis in A431 cells in real time. Furthermore, they demonstrated the possibility of lifetime discrimination between the fluorescence of SQDs and the largely overlapping fluorescence of Citrine in live cells. J. Conroy *et al.* investigated the mechanisms behind the tropism of TGA-capped CdTe to nuclei and nucleoli of THP1 cells, concluding that it may be mediated by the binding affinity of these SQDs to biopolymers within the nuclear compartments, such as core histones and nuclear lysates[116]. More recently, A. Orte *et al.*[84] used CdSe/ZnS SQDs as pH-sensitive fluorescent probes to visualise various intracellular regions in MC3T3-E1 and CHO-k1 cells (Figure 7).

2.6 Photostability

High photostability is one of the key requirements for a fluorescent label, especially for those applications requiring long acquisition time. In general, both SQDs and GQDs are considered to be very good in this regard, however, both can show photo-induced reduction[117–120] or enhancement[33,121–123] of fluorescence depending on the type of the quantum dot, the level of surface passivation and presence of any encapsulation layers. Neither of the

View Article Online
DOI: 10.1039/C8TB00153G

Table 2 Summary of optical properties of some synthesised graphene quantum dots

Probe type	D_{av} (nm) / height (nm)	Emission position	Shape of PL band	Excitation dependence	Stokes shift (nm)	Quantum Yield	Lifetime (ns)	Ref
COOH-GQD	7.1/—	490 nm	Asymmetric	Not stated	~100	3.9%		85
NH_2-GQD	6.3/—	440 nm	Asymmetric		~100	8.5%		
GQD	3.5/1.5	540 nm	Asymmetric	Yes	>60	9.2%		86
NH_2-GQD	4/—	440 nm	Asymmetric / shoulder	Yes	96	17.6%	5.7	83
GQD	4 / —	430 nm	Asymmetric / shoulder		92	20.4%	2.1	
PEG-GQD	60/2.5	510 nm	Asymmetric	Yes	110	3.8%		87
GQD	3/1.4	434 nm	Asymmetric	Yes	116		3.56	88
	6/1.4	500 nm	Asymmetric		169			
	9/1.4	564 nm	Asymmetric		135			
NH_2-GQD	3.8/2	540 nm	Almost symmetric	Yes	50	7%		33
$NHNH_2$-GQD	2.9/0.81	480 nm	Almost symmetric		70	45%	7.26	
OH-GQD	2.6/1.07	450 nm	Almost symmetric		80	21%		
GQD	9.6/1.5	430 nm	Symmetric	Yes	110	6.9%		67
GQD	4.5/—	510 nm	Extremely narrow peak	Not stated				89
PEG-GQD	6.6/1.5	420 nm	Slight shoulder	Not stated	90	4%		90
NH_2-GQD	6/—	429&497 nm	Double peak	Yes	>90	29%	~7	13
NH_2-GQD	2.5/1.1	420 nm	Slight asymmetry	Not stated		29%		32
	2.5/1.1	535 nm	Slight asymmetry			19%		
GQD	5.3/1.2	515 nm	Shoulder	Yes		11.4%		82
GQD	5/—	550 nm	Extremely narrow peak	Not stated	20			91
GQD	3/0.85	460 nm	Asymmetric	Yes	120			92
NH_2OH-GQD	3/0.85	420 nm	Asymmetric		105			
Pyrazole-GQD	3/0.85	550 nm	Asymmetric		100			
GQD	4/1.5	510 nm	Asymmetric	Yes	105			93
GQD	5/—	430&540 nm	Asymmetric / double peak	Yes	100	14%		94
GQD	4/0.75	445&503 nm	Double peak					95
GQD	3.1/1.3	475 nm	Asymmetric	Yes	130	1.2%		96
Carbide-GQD	3.1/1.3	440 nm	Almost symmetric		110	3%		
GQD	20/1.0	530 nm	Shoulder	Not stated	100			97
GQD	5.5/1.2	498 nm	Almost symmetric	Yes	98	11.7%		98
	6.8/1.2	540 nm	Asymmetric		120	4.8%		
	7.6/1.2	565 nm	Asymmetric		100	2.2%		
N-GQD	3/0.8	520 nm	Asymmetric / shoulder	Yes	130	31%	6.27	53
N-GQD	3.9/—	530 nm	Broad / shoulder	Yes	70			99
GQD	3/1.0	520 nm	Asymmetric	Yes		13.1%		100
N-GQD	5.3/—	520 nm	Almost symmetric	Yes	>100	8.4%		69
GQD	15/0.5	520 nm	Asymmetric	Yes	80	4.04%		101
	18/2.0	550 nm	Asymmetric		70	2.29%		
N-GQD	10.6/1.4	560 nm	Asymmetric	Yes	>100	9.1%		102
GQD	15/1.4	460 nm	Symmetric	Slight	~100	9%		103
PEG-GQD	13.3/—	440 nm	Slight shoulder	Yes	80	7.4%		70
N-GQD	4.5/1.2	500 nm	Asymmetric / shoulders	Yes	150	11.7%		104
	4.5/1.2	450 nm	Asymmetric / shoulders		115	22.9%		
GQD	4/1.5	473 nm	Asymmetric / shoulders	Not stated	>130			105
GQD	3/1.25	440 nm	Asymmetric / shoulders	Yes	80	10%		106
N-GQD	4/1.8	425 nm	Asymmetric / shoulders	Yes	>85			107
N-GQD	3.2/1.0	516 nm	Slight asymmetry / shoulder	Yes	100	6.0%	2.1 – 8.1	34
	3.6/2.0	446 nm	Slight asymmetry / shoulder		90	6.5%	2.7 – 3.5	
GQD	3.1/1	430 nm	Slight asymmetry / shoulder		90	12.1%	3.9 – 4.4	
N-GQD	3.5/—	425 nm	Asymmetric / shoulder	Yes	115	8.6%		71
GQD	4.2/1.5	458 nm	Multiple shoulders	Not stated	100	4.8%		108
N-GQD	3.8/1.5	440 nm	Almost symmetric / shoulder		125	23.3%		
N-GQD	4.5/—	705 nm	Extremely narrow peak	Yes	>250			43
N-GQD	5.8/1.7	302, 542 & 915 nm	Three distinct emissions All symmetric	Yes	105, 67 &107	11.3%	~1	44
NFS-GQD[a]	2/1.5	409, 435 & 465 nm	Triple peak	No		70%		68

[a] Sodium, Fluorine and Sulphur co-doped GQDs

View Article Online
DOI: 10.1039/C8TB00153G

effects is desirable for a fluorescent label, and thus the understanding of mechanisms of photo-induced fluorescence changes can aid in developing advanced synthesis method for the production of good-quality and highly-stable quantum dots.

In SQDs, the photo-induced reduction of fluorescence, or photo-bleaching, has been linked to irreversible photo-oxidation of the semiconductor material. The photo-oxidation causes a gradual decrease of the effective diameter of the core of the quantum dot, evidenced by a blue shift in its emission, and a formation of quenching states at the surface of the quantum dot with a subsequent reduction of the PLQY of the quantum dot[124,125]. On the other hand, photo-induced improvements of fluorescence in SQDs have been attributed to photo-annealing processes involving surface reconstructions[121,126]. Encapsulation of SQDs, for example in layers of silica material, has been shown to reduce photo-induced fluorescence changes[123,127]. For GQDs, no in-depth experimental investigations into the mechanisms of photo-induced fluorescence changes have been published to date; however, the vast majority of works quoting photostability data report no observable changes of GQD fluorescence with prolonged exposure[31].

3 Chemical properties

3.1 Synthesis of quantum dots

SQDs synthesis. A number of SQD types can be produced in aqueous environments to yield intrinsically water-soluble quantum dots: ZnS, PbS, CdS, CdTe, Cd_3As_2, Zn_3P_2, among others have been previously synthesised in this manner[128–135]. In essence, aqueous synthesis of SQDs can be thought of as a precipitation reaction between cation and anion precursors in the presence of a stabilising agent, which controls the precipitation process and limits the growth of the precipitate to nanometer-sized particles. Due to the relatively low temperature used during the reaction, these QDs tend to have moderate QYs (typically 40-50%), but do not require water-solubilisation treatments for applications such as fluorescent probes in biomedical applications. In fact, biomolecules such as proteins, nucleotides, nucleic acids and amino acids can be used as templates for the nanocrystal growth or as surface capping ligands, producing biofunctional SQDs in situ[136–139]. An excellent and extensive review of the aqueous methods of SQD synthesis was published recently by L. Jing *et al.*[128] and readers are directed to it for further details on the history and recent progress of aqueous synthesis methods, as well as the mechanisms of crystal growth, surface passivation techniques, doping methods and optical properties of SQDs prepared in such a manner.

Synthesis of highly fluorescent SQDs is usually achieved by organometallic chemistry involving pyrolysis of organometallic precursors in a hot coordinating solvent in the presence of stabilising ligands[140–143]. Pyrolysis of precursors causes supersaturation of constituent elements, and subsequent nucleation and growth of the semiconductor nanocrystals, with the stabilising ligands preventing the aggregation of nanocrystals into bulk semiconductor during the reaction. The high temperature of this method ensures removal of defects and passivation of surfaces during crystal growth, thus resulting in almost monodisperse, highly passivated SQDs. The subsequent epitaxial growth of an inorganic shell, composed from the semiconductor material of higher band-gap, further passivates the surface and from herein protects the core of the nanocrystal[144,145], resulting in very high QYs of SQDs grown by this method. However, application of these quantum dots in biomedical applications requires a further water-solubilisation treatment, which usually involves either an exchange of the stabilising ligands of SQDs for short-chain charged ligands or encapsulation of native SQDs in a layer of amphiphilic molecules[5,141,146]. In the case of the former, the passivation of the surface is usually somewhat reduced by the process, resulting in a pronounced decrease of the PLQY[147], however, the modified SQDs generally possess excellent solubility[22–24]. In the case of the latter, the native surface passivation remains untouched yielding superior PLQYs and stability of SQDs, however, the amphiphilic caps tend to be difficult to functionalise post-encapsulation[148], due to the 'bulkiness' of amphiphilic molecules used, yield large SQD with diameters greater than 25 nm[149].

GQD synthesis. While SQDs are always produced via a bottom-up method, both top-down and bottom-up approaches can be used for the production of GQDs. The bottom-up method, in this context sometimes referred to as carbonisation, involves pyrolysis of organic precursors, such as citric acid, glucose, pyrenes and polyphenylenes, using either thermal or microwave-assisted methods[33,35,69,87,98,103,108,151,152] (Table 3). Depending on the procedure and precursors used, some GQDs prepared by these methods may require further treatments to make them water-dispersible. However, this is easily achieved by mild oxidation. Top-down methods, on the other hand, involve exfoliation and/or cutting of carbon precursors, such as graphite[83,150], graphene[67,105], graphene oxide[71,86], carbon fibres[88,153], carbon black[101], fullerenes[92] and carbon nanotubes[68], through the use of reducing or oxidising agents. The cutting can be achieved either by hydrothermal[13,32,67,86,94,100], solvothermal[34,53,93,155], microwave-assisted[68,107] or electrochemical[90,102,104–106,150] (Table 3). All GQDs prepared by these methods are inherently water soluble and thus require no further treatments. Unfortunately, to date, no comprehensive studies have been published that critically assess the merit of each technique or the effect synthesis parameters have on the optical and chemical properties of prepared GQDs. As a result, as of this moment, there is no clear direction that can be pursued towards the development of a controlled synthesis method for fabrication of GQDs with pre-determined chemical and optical properties. This is both due to a rather limited amount of examples that exist in the literature, and a relatively wide breadth of methods that have been reported to date. Therefore, despite the fact that great advances have been made in this area in recent years, synthesis of GQDs is still complex and time-consuming.

3.2 Functionalisation and labeling strategies

Post-synthesis and solubilisation, QDs may undergo further chemical modifications, primarily aimed at achieving targeted ap-

View Article Online
DOI: 10.1039/C8TB00153G

Table 3 Synthesis methods for Graphene Quantum Dots

Probe type[a]	Synthesis method	Precursor	Ref
GQDs	Hydrothermal cutting and reduction	Graphene oxide	94
PEG-GQDs	Hydrothermal cutting and reduction	PEGylated graphene oxide	70
GQDs	Hydrothermal cutting and oxidation	Graphene oxide	86
Amino-GQDs	Hydrothermal cutting and exfoliation	Graphene oxide	13,32
N-GQDs	Hydrothermal cutting and exfoliation	Reduced graphene oxide	71
GQDs	Hydrothermal cutting	Graphene	67
GQDs	Electrochemical cutting	Graphene	105,106
N-GQDs	Electrochemical cutting	Graphene	107
GQDs, PEG-GQDs	Electrochemical cutting	MWCNTs	90
GQDs	Electrochemical oxidation	Graphite	150
GQDs, N-GQDs	Electrolysis	Graphite	102
GQDs, N-edge GQDs	Exfoliation and reduction	Graphite powder	83
GQDs, N-GQDs	Pyrolysis (acidic carbonisation)	Pyrene	33
GQDs	Pyrolysis (acidic carbonisation)	Polyaromatic hydrocarbons	98
GQDs	Pyrolysis (acidic carbonisation)	Dendritic polyphenylene	151
GQDs	Carbonisation (pyrolysis)	Citric acid	103
N-GQDs	Carbonisation (pyrolysis)	Citric acid	108,152
N-GQDs	Microwave-assisted hydrothermal pyrolysis	Glucose	44,53
GQDs	Controlled pyrolysis	Polyaromatic hydrocarbons	87
GQDs	Self-limiting pyrolysis	Polyaromatic hydrocarbons	35
GQDs	Oxidative cutting	Carbon fibres	88,89,91,153
GQDs	Oxidative cutting & exfoliation	Carbon black	101,154
GQDs	Oxidative cutting & exfoliation	Graphite	96,100
GQDs, PEG-GQDs	Oxidative cutting & exfoliation	Graphite	95
GQDs, N-edge GQDs	Oxidative cutting & exfoliation	Graphite	99
GQDs, N-edge GQDs	Cage opening (oxidative cutting)	Fullerene	92
N, F, S co-doped GQDs	Microwave-assisted cutting in ionic liquid	CNTs	68
N-GQDs	Microwave-assisted oxidative cutting	Graphene oxide	104
GQDs	Solvothermal cutting	Graphene oxide	82,93
GQDs, amino-GQDs	Solvothermal cutting	Graphene oxide	53
N-GQDs	Solvothermal cutting	Graphene oxide	34,155
GQDs	Photo-Fenton reaction	Graphene oxide	97

[a] GQDs refer to graphene quantum dots with oxygen-containing group at the edges (carboxyl, hydroxyl, *etc.*);
amino-GQDs refer to amino-functionalised GQDs; N-GQDs refer to nitrogen-doped GQDs;
N-edge GQDs refer to GQDs with N-containing edges and functional groups (predominantly not amino groups).

View Article Online
DOI: 10.1039/C8TB00153G

proaches for drug delivery and bioimaging. In addition, a suitably designed probe can have a higher internalisation, augmenting the efficacy of the delivered drug, providing higher contrast during bioimaging, significantly reducing the required dosages[31], as well as adding an additional modality to the system. Therefore, there is a requirement for fluorescent probes to have well-established libraries of functionalisation and labeling protocols. In this respect, both SQDs and GQDs offer many opportunities since both types of QDs usually have oxygenated and/or amino end-groups (post-synthesis and solubilisation). This allows for straightforward further modification of their chemistry using standard carbodiimide cross-linker reactions. For example, both X. Wang *et al.*[156] and Chun-Lin Huang *et al.*[157] have used carbodiimide chemistry to functionalise GQDs with folic acid, thus imposing specificity of their probes to folate receptor-overexpressing cancerous cells (e.g. HeLa), and similar examples also exist for SQDs of various compositions and shapes[58,158–161]. A further point to make is that attachment of molecular adaptors, such as streptavidin, avidin, and biotin, are also possible using same standard protocols, providing additional bioconjugation tools for ensuring specificity of the fluorescent probes[162]. In fact, it is now possible to procure commercial SQDs that are pre-labeled with molecular adaptors, greatly facilitating their implementation into differential bioimaging studies. A noteworthy recent development in the area of active targeting is a protocol for oriented conjugation of SQDs with single-domain antibodies to produce ultrasmall highly-specific fluorescent probes[61,62,163–166].

Non-covalent functionalisation or loading of QDs is also possible, for example, by using electrostatic assembly, hydrogen bonding, etc. In this case, however, the attachment of the loaded entities is not as strong and generally is found to be dependent on the chemical environment of the QD, leaving a possibility of them being detached from the surface upon a change in the environment. Indeed, in many cases, this fact has been exploited to achieve delivery and stimuli-responsive release of therapeutic drugs using quantum dots as traceable drug delivery systems.

For SQDs, the non-covalent attachment is usually based on an electrostatic attraction between the charged groups on their surface and an oppositely-charged biomolecule or drug. For example, Ellen R. Goldman *et al.*[167] showed that it is possible to electrostatically adsorb avidin to the surface of dihydrolipoic acid-modified SQDs, allowing for facile conjugation of biotinylated antibodies thereafter. Jianjiang Zhao *et al.*[168] used electrostatic assembly to attach survivin siRNA molecules to amino-PEG-SQDs for downregulation of survivin gene expression in oral squamous cell carcinoma cells, while Rijun Gui *et al.*[169] used the same method to load these type of SQDs with anticancer drug adrianycin for real-time monitoring of pH-dependent release of the drug in HeLa cells. In a slightly different approach to loading chemotherapy drugs to SQDs, Q. Yuan *et al.*[170] electrostatically-assembled ZnO SQDs with biodegradable chitosan – folic acid conjugates in the presence of Doxorubicin hydrochloride (DOX) drug, effectively trapping DOX in the SQD-chitosan-folic acid network. Upon a change of pH, the DOX drug was released from the network due to a shift in the equilibrium of positive and negative charges within the complex.

DOX is also a popular drug of choice for loading onto GQDs[93,156,157,171], although in this case the loading is typically performed via pi-pi stacking – staking of molecules based on attractive non-covalent forces between the aromatic rings contained within them. This ability of GQDs is of a great advantage since it facilitates loading of somewhat hydrophobic drugs onto GQDs without any modification of the drug, which simultaneously increases the drug's solubility in physiologically relevant media[172] and endows it with traceability. It can also impose a specificity to drug's delivery if GQD is pre-functionalised with a biorecognition element.

Furthermore, for both SQDs and GQDs, a combination of above methods can be used to develop highly multi-modal fluorescent probes. For example, Chun-Lin Huang *et al.*[157] used carbodiimide chemistry to graft onto GQDs an active targeting moiety in the form of folic acid, which imposed specificity of the probes to folate receptor-overexpressing cancerous cells. They also covalently attached a chelating agent for paramagnetic ions, in the form of diethlyene triamine penteaacetic acid, which enabled MR imaging ability of this platform. Finally, DOX was loaded onto the GQDs for the therapeutical purpose. In principle, in this manner, it is possible to develop theranostic agents that amalgamate any combination of the possible therapeutical properties (photodynamic, photothermal, chemotherapy) with a number of imaging capabilities (photoacoustic, photoluminescent, magnetic resonance).

3.3 Photoreactivity

In general, it is undesirable that a fluorescent probe undergoes any chemical changes or becomes chemically active in its environment upon photoexcitation. Such a property can, however, be exploited in the case where photoinduced chemical activity constitutes a production of reactive oxygen or other species that can attack and cause the destruction of cell membranes. In fact, Photodynamic Therapy (PDT) of cancer relies on exactly this process. The co-localisation of the drug, known as photosensitiser (PS), and a source of its photoexcitation results in increased selectivity of PDT compared to other therapies, with a consequential reduction of associated side-effects[173–176].

There are two main routes by which the highly reactive species can be produced upon excitation of PS. The first route, type I, involves an electron or hydrogen transfer and typically results in the production of charged reactive species such as superoxides and hydroxyl radicals. The second route (type II) is by triplet energy transfer (TET) between the PS and ground (triplet) state of the oxygen molecule, resulting in the production of highly reactive and cytotoxic singlet oxygen ($^1O_2$)[177–179]. It is generally accepted that singlet oxygen is primarily responsible for cell death in PDT[180,181] and, although contributions from species produced via the type I route are not negligible, it is customary to measure the efficacy of a PS drug by evaluating its singlet-oxygen yield[182]. Both SQDs and GQDs have been proposed for use as sensitisers in PDT of cancer. SQDs by themselves have been shown to produce ROS upon excitation but with efficiencies $\sim$10 times less than that of conventional PS drugs[183–185]. Furthermore, SQDs capable of generating ROSs tend to be of the core-only type, due

View Article Online
DOI: 10.1039/C8TB00153G

to the requirement of easy and close access of oxygen for charge and energy transfer from SQDs. Such SQDs are inherently less chemically and photo-stable compared to core-shell SQDs, and therefore, the lack of efficiency cannot be overcome by the argument of higher photostability of SQDs. A more promising approach in this area has been the employment of SQDs as a combinatory drug-carrier and light-harvesting system, in which a conventional PS drug is attached to the surface of the SQDs. In this configuration, the drug can be excited directly, depending on the wavelength used, but also through the non-radiative transfer of energy from SQDs. This effectively increases the overall absorption cross-section of the drug and the corresponding functional spectral range. Both electrostatic and covalent conjugates have been explored, involving type I and type II reactions, with reports of both increased and decreased efficiencies of ROS production [118–123,125–130]. The overall change in efficiency depends on the interplay between the possible photophysical interactions between the SQDs and the PS drug, i.e. the energy transfer and triplet-state quenching processes [186]. Even in the absence of efficient energy transfer, the use of SQDs as drug-delivery vehicles is a promising avenue, since their broad absorption bands allow the simultaneous visualisation of cancerous tissue and the photoactivation of the PS drug in a spectrally-independent manner.

Regarding GQDs, many works reference their use for PDT applications but these are usually in the context of multi-modal systems [187–191], where their use as PDT agents is in addition to other modalities such as a drug delivery carrier for a chemotherapy drug, as opposed to the inherent bi-modality of GQDs as imaging and PDT agents. In fact, very few works directly evaluate the efficiency of GQDs as PS drugs by measuring their singlet-oxygen yield. For example, Markovic *et al.* [150] and Jovanovic *et al.* [192] both used the Electron Paramagnetic Resonance measurements to monitor singlet-oxygen production by GQDs, however, neither compared their results to a traditional PS of known singlet oxygen yield. In majority cases where the performance of GQDs was compared to standard PSs, the rate of singlet oxygen generation by GQDs was determined to be significantly smaller [72,191,193]. Importantly, however, a relatively recent study by Ge *et al.* [194] found that the singlet oxygen yield of pristine GQDs can exceed that of the best performing traditional PSs. The key factor determining the efficiency of GQDs seems to be their functionalisation or encapsulation. For example, in their work on the use of GQDs as two-photon PDT agents, Kuo *et al.* [72] quote a value for 0.51 for the singlet oxygen yield of antibody-functionalised GQDs, which is significantly lower than the yield of 1.3 quoted in the study of Ge *et al.* [194]. Similarly, PEG-encapsulated GQDs produced by Chandra *et al.* [90] were found to produce considerably less ROSs compared to their un-capsulated counterparts, due to singlet oxygen quenching. These works infer a strong interplay between the effectiveness of GQDs as PSs and any chemical modification that they undergo to ensure a specificity of their delivery to cancerous tissues. An interesting approach to circumvent this issue could be the use of cleavable shells decorated with bio-recognition elements, similar to those used by Li *et al.* [195] for delivery and release of chlorine e6 from GQDs under a tumour relevant conditions. In general, however, more research is needed to quantitatively evaluate this link for different types of GQDs — only then the full potential of GQDs as PDT agents can fully be realised.

3.4 Chemical stability

In terms of the chemical stability, the requirement for fluorescence probes is one of stable fluorescence performance in the chemical environment that these probes are utilised in; thus, the pH of the medium, the temperature and the presence of any ions must be considered. This is particularly important for *in vivo* applications, where changes in fluorescent behaviour may be misinterpreted, and the chemical degradation of the probes can have direct detrimental effects. That being said, both SQDs and GQDs are colloidal materials, and as such are expected to have optimal regions of chemical environments for utilisation.

For example, the physical and chemical properties of SQDs drastically depend on the experimental conditions used, such as the pH of buffer solution used or bioconjugation reagents employed. The fluorescence of SQDs is known to be quenched under acidic conditions, such as those in cellular endosomes, and to be enhanced under basic conditions [196]. In the process of endocytosis, the exposure of amphiphilic polymer-encapsulated SQDs to the acidic environment in endosomes or lysosomes results in the spectral shift towards the blue region [197]. However, this instability can be resolved via surface modification strategies. For example, in a study by Hu *et al.* [196], CdSe/ZnS SQDs were functionalised with a silica and amphiphilic polymer, which resulted in a stable complex in a broad range of chemical conditions such as the strongly acidic environment. In their work, Hu *et al.* applied these stable SQD compounds in combination with a pH sensitive dye for pH sensing application, exemplifying how inherent instabilities of SQDs can be integrated into sensing schemes.

The SQDs with less than 5.5 nm hydrodynamic diameter are known to be rapidly cleared from the organism via urinary excretion; however, this is undesirable in biomedical application, such as drug delivery and bioimaging [198,199]. Functionalised SQDs, such as those typically employed for bioimaging application, are larger in hydrodynamic diameter than 5.5 nm and are uptaken via reticuloendothelial systems. As a result, they remain in the biological organisms for long periods of time [197], making their stability under physiological conditions a critical factor. Unfortunately, SQDs are known to be quite unstable under certain physiological, chemical and environmental conditions, halting their full application for *in vivo* diagnostics and quantitative imaging. This is of particular concern in view of the fact that most of the SQDs are composed of carcinogenic compounds, such as Cd, the release of which upon degradation may result in potentially high toxicity [200], although this is disputed among the research community (see next section). Nonetheless, functionalisation strategies involving small molecule ligands [201], and amphiphilic polymers [136,202–204], as well as encapsulation strategies using silica material [205–209], have all been previously employed in order to make SQDs more soluble and stable in physiologically relevant solutions.

Similarly to SQDs, and in the reflection of their colloidal nature, GQDs are also generally reported to have fluorescence properties

View Article Online
DOI: 10.1039/C8TB00153G

and aggregation behaviour dependent on the pH and temperature of their solutions, as well as the presence of ions in their environment[31]. An interesting contrast to point out here is that the latter dependency is somewhat selective to the types of ions present. A study published by Li *et al.*[153] investigated the stability and aggregation kinetics of GQDs in different buffer conditions (i.e., cation type/valence, pH values, and the combined effect of cations and pH). The author has demonstrated that the presence of divalent cations, such as Mg^{2+} and Ca^{2+}, resulted in increased aggregation of GQD plates, reflected in a negative nonlinear correlation between a quantitative indicator for the evaluation of the stability of NPs in aqueous solution – the critical coagulation concentration and pH values. In contrast, the monovalent cations such as Na^{2+} and K^{+} did not affect GQD stability, and the positive linear correlation was observed between the critical coagulation concentration and pH levels. In their work, the authors have proposed a three-step mechanism of aggregation of GQDs in the presence of divalent cations.

Another study by Guo *et al.*[210] utilised rhodamine B derivative-functionalized (RBD) GQDs for detection of Fe^{3+} ion *in vitro*, the accumulation, and deficiency of which is known to lead to a number of health problems such as anaemia, cancers, and organ dysfunction[211,212]. The application of RBD-GQDs as Fe^{3+} turn-on nanosensor in living cells was based on a fluorescence enhancement effect in the presence of Fe^{3+} ions. The effect of several other ions was also investigated, some of which were physiologically significant (Ca^{2+}, Fe^{2+}, K^{+}); however, these did not show a similar enhancement effect. Overall, the RBD-GQD complexes were shown to have increased water solubility, sensitivity, biocompatibility, and photostability, when compared to Rhodamine B dye under similar conditions.

4 Biocompatibility

Biocompatibility is perhaps the most important property of a newly-developed material when considering its utilisation for biomedical applications. It is usually evaluated by considering the cytotoxicity (*in vitro* toxicity) of the material and through *in vivo* studies that look at biodistribution, clearance routes and longterm side effects post-injection. Biocompatibility is a highly complex property that cannot be fully predicted based on the composition of the material. For many colloidal nanomaterials, factors such as nanoparticle size, shape, aspect ratio, surface functionalisation, encapsulation layers, presence of external excitation source and (especially) dose have all been found to have a profound effect. This makes the direct comparison between the biocompatibilities of SQDs and GQDs extremely difficult. Therefore, the first two subsections of this discussion mainly focus on key findings for the two types of QDs regarding their *in vitro* and *in vivo* toxicities. The last subsection attempts to provide a more direct point of reference from which to view these results, by comparing the limit of detection for confocal imaging applications and relating it to the dose of QDs used in the toxicity studies.

4.1 Toxicity *in vitro*

A number of biocompatibility studies have been carried for both SQDs and GQDs. With respect to the former, the toxicity of commonly used SQDs has raised a lot of concern due to the intrinsic toxicity of such Cd-containing quantum dots. Consequently, recent years saw a shift in the scientific focus towards the development of non-heavy metal based SQDs or their encapsulation in protective layers, both of which have shown reduced toxicity[127,205,213,214]. On the other hand, the demand for safer alternatives generated interest in carbon-based nanoprobes, including graphene quantum dots, which promised intrinsic biocompatibility. However, some types of GQDs have been shown to be highly photoreactive causing damage on a cellular level, but elucidating that, independent of the intrinsic nature of the material used, the toxicity of the final product is also dependent on other factors such as surface modification, size, shape, dosage, and delivery method[10].

Another contributor to SQD's toxicity *in vitro* and *in vivo* is the free radical generation, such as singlet oxygen, hydroxyl radical ($^{\cdot}OH$), superoxide anion ($^{\cdot}O_2$), hydrogen peroxide (H_2O_2), and peroxynitrite ($^{\cdot}ONOO$). SQDs are extremely photosensitive and are known to transfer the energy to molecular oxygen forming singlet oxygen, which reacts with water and catalyses the enzymatic reaction in order to produce reactive oxygen or nitrogen species (ROS/RNS)[215,216]. The free radicals can cause damage not only on the cellular level (cell apoptosis) but can also lead to mutations in the DNA[217,218]. Some consider oxidative stress to be the primal cause of toxicity of QDs *in vitro*. However, this production of singlet oxygen can also be used to an advantage, where this particular property showed potential in the application of PDT for a more targeting cancer therapy[219–221], as discussed previously. In an attempt to reduce the toxicity of SQDs, shell coating method has been applied on numerous occasions which, as the name suggests, involves coating of SQD cores with shells of another inorganic material (e.g. ZnS), small molecules, polymers, proteins or silica[9,127]. The coatings allow for a slower transport of oxygen to the core surface thus reducing the rate of ROS production, however, they do not completely inhibit it and they tend to be susceptible to degradation in the cellular environment.

GQDs, on the other hand, were first considered because of their intrinsic low toxicity owing to their carbon-based compositions[222], and they have since become an attractive target for biomedical applications. However, even though GQDs have been shown to have quite a low toxicity, it is not altogether absent. Several *in vitro* studies were performed in order to evaluate the cytotoxicity of GQDs and some of these can be found summarized in Table 4. The most commonly cited origin of cytotoxicity in GQDs is the photoinduced production of reactive oxygen species, such as superoxide anions and singlet oxygen[223,224]. Production of ROS has been linked to induced cytotoxicity and cell death (apoptosis) via activation of a group of cysteine proteases called caspases[225,226]. The oxidative stress and the damage caused within the cells can, in turn, promote increased autophagy in order to clear damaged cellular components. This is the first line of defence for cells in case of nanoparticle-induced cytotoxicity[227].

View Article Online
DOI: 10.1039/C8TB00153G

Table 4 *In vitro* cytotoxicity studies using graphene quantum dots

Probe type[a]	Cytotoxicity test(s)	Length of exposure	Cell type	Results	Ref.
PEGylated GQDs	WST-1, LDH	24 hr		No indication of toxicity;	95
			HeLa	95% viability at 160 μg.mL^{-1}	
			A549	85% viability at 640 μg.mL^{-1}	
GQDs and hydrothermally treated GQDs	WST-1	24 hr	A549	~80% viability at 100 μg.mL^{-1}	96
GQDs	MTT	24 hr	MCF-7	>80% viability at 200 μg.mL^{-1}	97
			MGC-803	>70% viability at 200 μg.mL^{-1}	
GQDs (from pyrene)	MTT	24 hr	MCF-7	100% viability at <100 μg.mL^{-1}	98
				>90% viability at 500 μg.mL^{-1}	
N-doped GQDs	Cell viability	24 hr	HeLa	~80% viability at 400 μg.mL^{-1}	53
GQDs (rich in N and O groups)		24 hr	RSC96	>90% viability at 0-100 μg.mL^{-1}	85
				>60% viability at 300 μg.mL^{-1}	
GQDs	MTT	24 hr	RSC96	>90% viability at 100 μg.mL^{-1}	82
				>80% viability at 400 μg.mL^{-1}	
N-GQDs	SEIRA	20 min	RBC	At 50 μg.mL^{-1} disturbance of order and conformation of lipid, possibly due to incorporation of GQDs, resulting in formation of echinocytes	155
GQDs	MTT	24 hr	THP-1	>93% viability at 0-100 μg.mL^{-1}	100
				82.5% viability at 200 μg.mL^{-1}	
		48 hr		>92% viability at 0-10 μg.mL^{-1}	
				87.3% viability at 50 μg.mL^{-1}	
				76.1% viability at 100 μg.mL^{-1}	
				62.2% viability at 200 μg.mL^{-1}	

[a] Unless otherwise stated, GQDs were used as-prepared and contained the native oxygenated edges (carboxyl, hydroxyl, *etc*.)

In addition, it has been previously shown that cells exposed to QDs express higher levels of L3B-II protein, which is a marker for autophagy[150,228]. Analogous to the similar issue with SQDs, attempts have been made to reduce ROS-related cytotoxicity of GQDs through surface modification or encapsulation of GQDs in protective layers. For example, crude GQDs were found to be more cytotoxic compared to PEG-functionalised GQDs. This reduced toxicity could be a combined effect of PEG being more biocompatible and the larger size of PEG-GQDs[90].

In the area of gene expression and genotoxicity, some detailed research has been carried out for SQDs concluding that long exposure to SQDs can lead to DNA damage, resulting in DNA mutation and possibly leading to cancer and other side-effects[209,231]. However, only a limited number of studies were carried out examining genotoxicity effect of GQDs. The only study to date that looked at genotoxicity of GQDs has been that of C. Wu *et al*., in which flow cytometry and cell cycle analysis of MCF-7 and MGC-803 cells was used to demonstrate some damage to GQDs[97]. This area urgently requires further investigations if GQDs are to be considered for medical applications.

Another area that somewhat falls short on the scope and detail of available information is that of cytotoxicity studies on cells that are involved in inflammation, such as macrophages. This is of particular importance for GQDs, as their counterparts graphene and graphene oxide have been shown, in mice, to result in pulmonary inflammation upon inhalation[232,233]. Even though the level of resultant inflammation can be reduced through functionalization of GQDs, the need for more detailed *in vitro* and *in vivo* studies on cytotoxicity of GQDs is evident. Only one study exists that investigated the effect of GQDs on macrophage cell line THP-1 by Qin *et al*., demonstrating that in activated THP-1 cells GQDs result in induced ROS generation, increased apoptosis, autophagy, and inflammatory response via p38MAPK and NF-kB mediated signaling pathways[100].

In general, for both types of quantum dots, the cytotoxicity results point to strong dependencies on a number of parameters, with favourable outcomes for quantum dots of either type encapsulated in protected layers and at reduced doses. For SQDs, the main concern is the presence of Cd ions – a point which may be rendered mute by the development of cadmium-free SQDs. For GQDs, the main concern at the moment is lack of information, although this is slowly being addressed with key dependencies being gradually established. A recent review by S. Wang *et al*.[234] neatly summarises some of these results, and the readers are directed to it for further information.

4.2 Toxicity *in vivo*

One of the unique property of nanoparticles is that, due to their small size, they are able to access the areas within a cell or body that are difficult to penetrate. For example, nanoparticles that are less than 100 nm in size can enter the cell, those that are less than 40 nm can enter the nucleus of the cell and those that are less than 35 nm can cross the blood-brain barrier[235]. Both types of quantum dots are very small in size and can easily cross the blood-brain barrier, which can potentially lead to severe side-effects[236]. Consequently, detailed *in vivo* toxicity studies are absolutely crucial; yet, only a limited number of studies have looked at *in vivo* toxicity of SQDs and GQDs.

Perhaps one of the more comprehensive studies involving SQDs has been one of Hauck *et al*.[229], where an assessment of *in vivo*

View Article Online
DOI: 10.1039/C8TB00153G

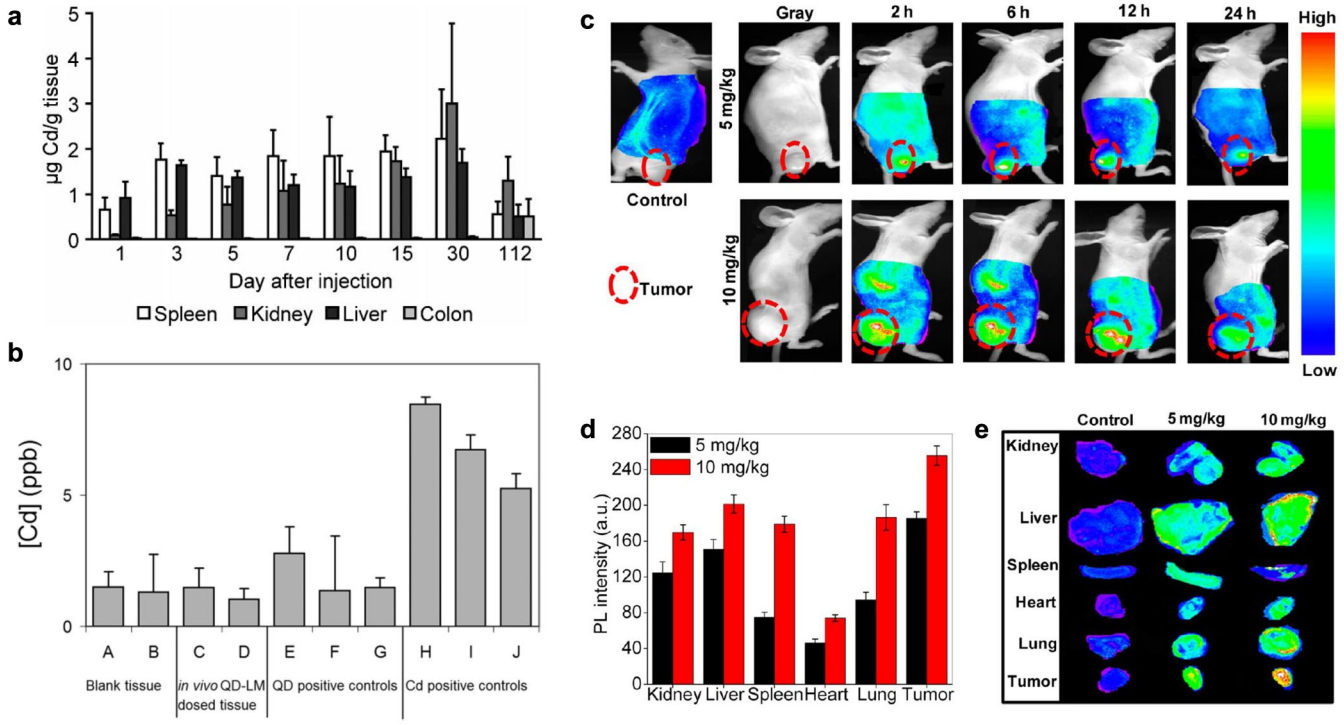

Fig. 8 Biodistribution of semiconductor (a,b) and graphene (c-e) quantum dots in mice. (a) Biodistribution of carboxyl CdSe/ZnS quantum dots in Sprague-Dawley rats, deducted from levels of Cd in the tissue. Reprinted with permission from Hauck *et al.*[229] Copyright (2017) John Wiley and Sons. **(b)** Digestion and ultracentrifucation studies of CdSe/ZnS studies in Sprague Dawlet rats, showing ACP-AES signal of spleen (A, C, F and I), liver (B, D, G and J) in tissue (A-D), with (A, B) and without (C, D) prior dosing of quantum dots and in positive controls (SQDs in PBS buffer: E-G and Cd spiked aqueous solution: H-J). Reprinted with permission from H. C. Fischer *et al.*[230] Copyright (2017) John Wiley and Sons. **(c-e)** Biodistribution of carboxylated GQDs in Balb/c nude mice (c) *in vivo*, at various times post-injection, (d) 2 hours post-injection from isolated organs, and (e) ex-vivo, 24 hours post-injection into tomour site, monitored via GQD fluorescence. Reprinted with permission from M. Nurunnabi *et al.*[89] Copyright (2017) American Chemical Society.

toxicity was carried out for CdSe-ZnS core-shell QDs with different surface functionalization groups, using female Sprague-Dawley rats as *in vivo* model. In this study, several toxicity indicators were examined, including animal survival, biodistribution, animal mass, haematology, clinical biochemistry, and organ histology over short and long periods of time (>80 days). The study showed that, in the short-term, SQDs accumulate primarily in the spleen and liver, as is expected during clearance from the blood by cells of the mononuclear phagocytic system; after several weeks, the authors hypothesised, SQDs partially break down into their constituent elements, causing the accumulation of Cd in the kidneys (Figure 8a). This is a point of worry, since the heavy metal ions, such as Cd^{2+}, released in the process degradation of SQDs are known to bind to heavy molecular weight proteins, such as metallothionein. The clearance of these protein-heavy metal ion complexes from the organism is a very slow process; for example, metallothionein-Cd complexes were shown to have a biological lifetime in the kidney of 38 years[237]. However, Hauck *et al.* concluded that the levels of Cd accumulation observed in their study were insufficient to cause any significant toxicity.

In another study, H. C. Fischer *et al.*[230] have examined biodistribution, sequestration, and clearance of CdSe-ZnS SQDs in the same rat *in vivo* model. They found that the short-term biodistribution of SQDs depended strongly on their functionalisation, with bovine serum albumin-conjugated SQDs being uptaken quicker by the liver than those that were stabilised by mercaptoundecanoic acid cross-linked with lysine. Interestingly, they did not observe degradation of the SQDs, unlike the study mentioned above, nor were they excreted in the short term (Figure 8b), suggesting that SQDs are sequestered and later re-distributed *in vivo*.

Concerning GQD's *in vivo* toxicity, there is a rather underwhelming amount of works on this subject and the results are often contradictory to each other, perhaps in reflection of the vast amount of dependencies that biocompatibility has on different nanoparticle parameters. By far the two most comprehensive studies of *in vivo* toxicities of GQDs were performed by Nurunnabi *et al.*[89] and Chong *et al.*[95], both opting to use Balb/c mice for their studies. Nurunnabi *et al.* used carboxylated GQDs synthesised by exfoliation of carbon fiber in acid and injected intravenously, while Chong *et al.* use Cy-7-labelled PEGylated GQDs synthesised by oxidative cutting from graphite and injected either intravenously or interperitoneally. While Chong *et al.* observed no differences in biodistribution depending on injection site, there were vast differences in biodistribution between the two types of GQDs. The PEGylated GQDs, injected at a dose of 15 $mg.kg^{-1}$ accumulated primarily in kidneys with low levels of fluorescence reported for all other organs and the tumour site. On the other hand, the biodistribution of carboxylated GQDs was more even

View Article Online
DOI: 10.1039/C8TB00153G

across all organs (Figure 8c-e), with a significant proportion being accumulated in the tumour site. Furthermore, the proportion of GQDs accumulating in spleen and lung increased significantly at a higher dose of 10 mg.kg^{-1} (when compared to 5 mg.kg^{-1}). This is worrying since the former could impact the modulation of the immune system and the latter could lead to pulmonary inflammations, as was previously observed for GQDs' counterparts graphene oxide[222,238].

The clearance of GQDs from body was not well reported by Nurunnabi *et al*. who do not provide any data apart from time-stamped *in vivo* images (Figure 8c) and noting that the fluorescence signal decreased to non-observable levels in 24 hours and that fluorescence levels of *ex vivo* images of dissected organs at 24 hours post-injection were lower than those at 12 hours post-injection. They attribute that to the excretion of GQDs from the body but do mention that loss of fluorescence in time could also be a factor. Indeed, as GQDs partly consist of aromatic carbons, their metabolism cannot be ignored as a possible source of loss of fluorescence. However, the authors make no attempts to resolve this issue.

Chong *et al*. do provide trends for all major organs for the duration of their study (48 hours). The results show a rapid clearance of GQDs from kidneys. This result, combined with significant levels fluorescence in the urine and its absence in the reticuloendothelial system, led to the conclusion of fast metabolism through kidneys as the main mechanism of body clearance for PEGylated GQDs. However, one issue that the authors do not discuss is the trends observed for other organs. Specifically, the fact that fluorescence levels in liver, heart and lung remain more or less constant over the 24 hours, while those in spleen seem to increase over the same time period. These facts suggest that a proportion of GQDs is sequestered and then redistributed. Given the short length of the study one cannot rule out this possibility, or the possible long-term side-effects due to the presence of these GQDs in the spleen.

Both studies did perform long-term haematological and biochemical blood analysis, with tests conducted over periods of 22 and 40 days, with injections every other day over first 14 days at a dose of 5 and 10 mg.kg^{-1} and 20 mg.kg^{-1} respectively by Nurunnabi *et al*. and Chong *et al*. Both report all marker levels within normal ranges and no indicators of any obvious toxicity. Similarly, both report no major histopathological abnormalities and legions for the two types of GQDs, with the exception of moderate pathological changes in the liver and lung for carboxylated GQDs at 21 days post-injection for the 10 mg.kg^{-1} dose. These results do suggest low *in vivo* toxicity of GQDs, especially those that are encapsulated. However, they also highlight the differences between GQDs depending on some basic parameters (such as size, functionalisation and dose) and call for further longterm studies involving different types of GQDs so that a full understanding of GQD uptake, biodistribution, toxicity and clearance can be developed.

4.3 Comparison of limits of detection

When performing confocal imaging of live animals or tissues, the limit of detection (LOD) relates to the minimum signal that must reach the detector to be able to distinguish it from the background (e.g. autofluorescence). In general, the detected signal will depend on: the attenuation of excitation source by tissues, the probe's (linear or nonlinear) absorption coefficient at the excitation wavelength, the concentration or amount of the probe that is excited (i.e. dosage), the PLQY of the probe, the attenuation of the emitted signal by tissues, and the detector efficiency at the emission wavelength. For the sake of a more direct comparison between the probes, the latter is assumed to be the same across the considered below spectral range. We further limit our discussion to typical QD samples, i.e. those that can be considered representative of each QD type. For SQDs, this is a sample that emits at 655 nm with PLQY of ~75 %, and has a Stokes' shift of ~50 nm, yielding the optimal excitation wavelength of 600 nm and a corresponding extinction coefficient of ~3x10^5 M^{-1} cm^{-1} (according to Peng *et al*.[88]). For GQDs, this is a sample emitting at 520 nm with ~10 % PLQY and 100 nm Stokes' shift, yielding the optimal excitation wavelength of 420 nm. The extinction coefficient of GQDs is taken to be same as that for the SQD sample since the extinction coefficients of GQDs are not well reported, but those few that are reported are in the same range as those of SQDs (Table 1).

Considering only the photophysical properties of the quantum dots, the signal that can be obtained with SQDs is 7.5 times larger than if using GQDs at the same concentration. However, the attenuation of the excitation source by tissues at the optimal excitation wavelength for GQDs (420 nm) is ~20 times stronger when compared to that at the optimal excitation wavelength of SQDs (600 nm), using breast tissue as an example[239]. Similarly, the emitted signal will also be attenuated ~5 times more at the wavelength of GQD emission (520 nm) compared to attenuation at the wavelength of SQD emission (650 nm). Therefore, for equal excitation powers, probe concentrations and detector efficiencies, the fluorescence signal detected when using GQDs as *in vivo* bioimaging probes will be almost three orders of magnitude lower (~750).

This has implications for the LOD for bioimaging: to obtain the same level of contrast during imaging, the dose requirement for a typical GQD sample is three orders of magnitude larger than that for a typical SQD sample. Using an LOD value for SQDs emitting at 655 nm reported by M. Roy *et al*.[240] (0.57 pmol.g^{-1}, or a dose of ~0.5 mg.kg^{-1}), the GQD dose required to achieve the same level of contrast would be 35 mg.kg^{-1}, taking into account their lower molar weights (~10 times lower than SQDs). Importantly, this value is higher than those considered in toxicity studies in the section above; and for practical applications, doses even larger that this will need to be used. Therefore, despite the very rough nature of these estimates, one can argue that most of the toxicological studies involving GQDs are not appropriate to be able to draw any deterministic conclusions regarding their longterm *in vivo* toxicity, as the dosages used are less than those required for practical applications.

View Article Online
DOI: 10.1039/C8TB00153G

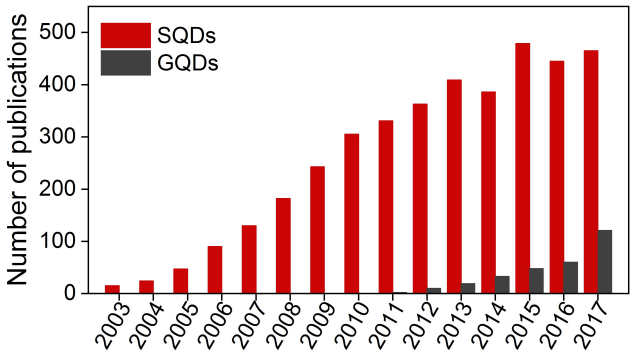

Fig. 9 Number of publications on the use of QDs for cancer therapy and diagnosis. Statistics were taken from Web of Science searches on the topic, including either SQD (red) or GQDs (black) as keywords.

5 Conclusions

Although inherently of very different nature, both types of QDs are attractive candidates for utilisation as fluorescence labels for diagnosis and therapy of cancer. Their distinguishing physiochemical properties make each type of QDs more suitable to specific applications or determine the mode of their implementation to achieve a specific task. For example, the symmetric and size-dependent photoluminescence band of SQDs, combined with extremely wide absorption bands make them ideal candidates for multiplexing applications. This would be difficult to achieve with the quasi-molecular fluorescence of GQDs that tends to be excitation wavelength dependent. On the other hand, pristine GQDs are excellent producers of ROSs and thus show great potential for photodynamic therapy applications.

However, despite their considerable promise, a number of issues remain to be addressed. For example, for SQDs there exists a number of well-developed synthesis methods and an extensive library of functionalisation and labelling protocols. However, typical PLQYs of cadmium-free SQDs remain to be quite low and very few of these have emissions in the NIR – there is an urgent need to develop efficient synthesis methods for this type of SQDS. Another area that somewhat deficient in examples is that of multiplexed applications of SQDs – this is surprising since SQDs are ideal candidates for such mode of utilization. Furthermore, both graphene and semiconductor QDs lack characterisation in terms of their nonlinear properties and their photoreactivity. This is an issue because new probes such as QDs can be considered for real-life applications only when all interdependencies between the physical and chemical properties of QDs have been identified. This is particularly problematic for GQDs, for which there is a general lack of information on a number of fronts, including their key optical properties (PLQYs, extinction coefficients, lifetimes etc.), mechanisms of photobrightnening and photobleaching, the interrelation of optical properties to synthesis method and mechanism of ROS generation. However, GQDs are relative new-comers to the field and the rate of publications on their use for cancer therapy and diagnosis is increasing quickly, unlike that of SQDs which seems to have saturated over the last few years (Figure 9). It is thus expected that many of the knowledge gaps mentioned above will be addressed.

A final note that we would like to make here relates to the lack of toxicity information for both types of quantum dots. This is a worrying factor that urgently needs addressing. Any application of QDs for biomedical purposes is prerequisite upon an extensive study of their biocompatibility and cytotoxicity. Unfortunately, there is no standardised methodology for such assessment that currently exists and it is, therefore, impossible to compare results obtained from different biomedical applications that can be found in the literature. This is of note because the toxicity of the vast range of nanomaterials used in literature has been shown to depend heavily on their composition, size, and methods of delivery, shape, chemical structure, surface properties such as charge, biodistribution, biodegradation, and many more. In this respect, the functionalization of QDs should consider the target and route of administration, i.e. intravenous or oral, and adjust the functionalization process accordingly. Depending on the size, surface functionalization, charge and hydrophobicity QDs may elicit different immune reactions. For cancer therapy applications, the effect of QDs in terms of cytotoxicity should be studied both in cancerous tissues and in normal cells that may come in contact with QDs on their route to the target, and in terms of the effect of their excretion in exosomes after drug release. Furthermore, the cytotoxicity should be studied over a long-term exposure since any long-term cytotoxicity may lead to disruption of normal bodily functions on a cellular level and may eventually result in disease or other side-effects, even if QDs are not toxic immediately following administration. Finally, the photophysical properties of the probes need to be considered when determining the appropriate dosage ranges for toxicity studies.

Conflicts of interest

There are no conflicts of interest to declare.

Acknowledgements

The authors would like to acknowledge the financial support of the Royal Society (UF150542). They also thank K. Crosbie-Staunton for his support, encouragement and the many helpful comments on the manuscript.

References

1 N. Triggle, Half of cancer sufferers 'live a decade or more', *http://www.bbc.co.uk/news/health-27194823*, 2014, (accessed 1 January 2017),.

2 Cancer Research UK, *http://www.cancerresearchuk.org/health-professional/cancer-statistics/*, 2017, (accessed January 1 2017).

3 D.-E. Lee, H. Koo, I.-C. Sun, J. H. Ryu, K. Kim and I. C. Kwon, *Chem. Soc. Rev.*, 2012, **41**, 2656–2672.

4 U. Resch-Genger, M. Grabolle, S. Cavaliere-Jaricot, R. Nitschke and T. Nann, *Nature methods*, 2008, **5**, 763–775.

5 Mostafa a. El-Sayed, *Accounts of Chemical Research*, 2004, **37**, 326.

View Article Online
DOI: 10.1039/C8TB00153G

6 K. D. Wegner and N. Hildebrandt, *Chemical Society reviews*, 2015, **44**, 4792–834.

7 A. Mukherjee, Y. Shim and J. Myong Song, *Biotechnology Journal*, 2016, **11**, 31–42.

8 S. A. O. Gomes, C. S. Vieira, D. B. Almeida, J. R. Santos-Mallet, R. F. S. Menna-Barreto, C. L. Cesar and D. Feder, *Sensors*, 2011, **11**, 11664–11678.

9 C. E. Bradburne, J. B. Delehanty, K. Boeneman Gemmill, B. C. Mei, H. Mattoussi, K. Susumu, J. B. Blanco-Canosa, P. E. Dawson and I. L. Medintz, *Bioconjugate chemistry*, 2013, **24**, 1570–83.

10 Y. Wang, R. Hu, G. Lin, I. Roy and K. T. Yong, *ACS Applied Materials and Interfaces*, 2013, **5**, 2786–2799.

11 A. Cayuela, M. L. Soriano, C. Carrillo-Carrión and M. Valcárcel, *Chemical Communications*, 2016, **52**, 1311–1326.

12 K. a. Ritter and J. W. Lyding, *Nature materials*, 2009, **8**, 235–42.

13 G. S. Kumar, R. Roy, D. Sen, U. K. Ghorai, R. Thapa, N. Mazumder, S. Saha and K. K. Chattopadhyay, *Nanoscale*, 2014, **6**, 3384–3391.

14 S. Schumacher, *Physical Review B - Condensed Matter and Materials Physics*, 2011, **83**, 1–4.

15 L. Cao, M. J. Meziani, S. Sahu and Y. P. Sun, *Accounts Of Chemical Research*, 2013, **46**, 171–180.

16 Z. Z. Zhang, K. Chang and F. M. Peeters, *Physical Review B - Condensed Matter and Materials Physics*, 2008, **77**, 235411.

17 J. Jasieniak, L. Smith, J. v. Embden, P. Mulvaney and M. Califano, *Journal of Physical Chemistry C*, 2009, **113**, 19468–19474.

18 W. W. Yu, L. Qu, W. Guo and X. Peng, *Chemistry of Materials*, 2003, **15**, 2854–2860.

19 P. N. Prasad, *Nanophotonics*, John Wiley & Sons, Inc., 2004, ch. 4, pp. 79 – 127.

20 G. d. A. Farias and J. S. de Sousa, *Handbook of Nanophysics: Nanoparticles and Quantum Dots*, CRC press, 2011, ch. 35, pp. 1–16.

21 E. E. Vdovin, A. Levin, A. Patanè, L. Eaves, P. C. Main, Y. N. Khanin, Y. V. Dubrovskii, M. Henini and G. Hill, *Science*, 2000, **290**, 122–124.

22 M. G. Bawendi, M. L. Steigerwald and L. E. Brus, *Annual Review of Physical Chemistry*, 1990, **41**, 477–496.

23 O. Voznyy, *Journal of Physical Chemistry C*, 2011, **115**, 15927–15932.

24 M. Yu, G. W. Fernando, R. Li, F. Papadimitrakopoulos, N. Shi and R. Ramprasad, *Applied Physics Letters*, 2006, **88**, 231910.

25 A. H. Ip, S. M. Thon, S. Hoogland, O. Voznyy, D. Zhitomirsky, R. Debnath, L. Levina, L. R. Rollny, G. H. Carey, A. Fischer, K. W. Kemp, I. J. Kramer, Z. Ning, A. J. Labelle, K. W. Chou, A. Amassian and E. H. Sargent, *Nature Nanotechnology*, 2012, **7**, 577–582.

26 Q. Wang, Y. Xu, X. Zhao, Y. Chang, Y. Liu, L. Jiang, J. Sharma, D. K. Seo and H. Yan, *Journal of the American Chemical Society*, 2007, **129**, 6380–6381.

27 A. Nourbakhsh, M. Cantoro, T. Vosch, G. Pourtois, F. Clemente, M. H. van der Veen, J. Hofkens, M. M. Heyns, S. De Gendt and B. F. Sels, *Nanotechnology*, 2010, **21**, 435203.

28 T. Gokus, R. R. Nair, A. Bonetti, M. Böhmler, A. Lombardo, K. S. Novoselov, A. K. Geim, A. C. Ferrari and A. Hartschuh, *ACS Nano*, 2009, **3**, 3963–3968.

29 M. L. Mueller, X. Yan, J. A. McGuire and L. S. Li, *Nano Letters*, 2010, **10**, 2679–2682.

30 D. Pan, L. Guo, J. Zhang, C. Xi, Q. Xue, H. Huang, J. Li, Z. Zhang, W. Yu, Z. Chen, Z. Li and M. Wu, *Journal of Materials Chemistry*, 2012, **22**, 3314–3318.

31 K. L. Schroeder, R. V. Goreham and T. Nann, *Pharmaceutical Research*, 2016, **33**, 2337–2357.

32 H. Tetsuka, R. Asahi, A. Nagoya, K. Okamoto, I. Tajima, R. Ohta and A. Okamoto, *Advanced Materials*, 2012, **24**, 5333–5338.

33 L. Wang, Y. Wang, T. Xu, H. Liao, C. Yao, Y. Liu, Z. Li, Z. Chen, D. Pan, L. Sun and M. Wu, *Nature communications*, 2014, **5**, 5357.

34 S. Zhu, J. Zhang, S. Tang, C. Qiao, L. Wang, H. Wang, X. Liu, B. Li, Y. Li, W. Yu, X. Wang, H. Sun and B. Yang, *Advanced Functional Materials*, 2012, **22**, 4732–4740.

35 X. Yan, X. Cui, B. Li and L. S. Li, *Nano Letters*, 2010, **10**, 1869–1873.

36 J. Mao, J.-N. Yao, L.-N. Wang and W.-S. Liu, *Journal of Colloid and Interface Science*, 2008, **319**, 353–356.

37 Y. Ebenstein, T. Mokari and U. Banin, *Applied Physics Letters*, 2002, **80**, 4033–4035.

38 A. B. Greytak, P. M. Allen, W. Liu, J. Zhao, E. R. Young, Z. Popović, B. J. Walker, D. G. Nocera and M. G. Bawendi, *Chemical Science*, 2012, **3**, 2028–2034.

39 J. McBride, J. Treadway, L. C. Feldman, S. J. Pennycook and S. J. Rosenthal, *Nano*, 2006, **6**, 1496–1501.

40 B. Mahler, P. Spinicelli, S. Buil, X. Quelin, J.-P. Hermier and B. Dubertret, *Nature Materials*, 2008, **7**, 659–664.

41 O. Chen, J. Zhao, V. P. Chauhan, J. Cui, C. Wong, D. K. Harris, H. Wei, H.-S. Han, D. Fukumura, R. K. Jain and M. G. Bawendi, *Nature materials*, 2013, **12**, 445–51.

42 A. M. Smith, M. C. Mancini and S. Nie, *Nature Nanotechnology*, 2009, **4**, 710–711.

43 M. Nurunnabi, Z. Khatun, G. R. Reeck, D. Y. Lee and Y.-k. Lee, *Chemical communications*, 2013, **49**, 5079–81.

44 L. Tang, R. Ji, X. Li, G. Bai, C. P. Liu, J. Hao, J. Lin, H. Jiang, K. S. Teng, Z. Yang and S. P. Lau, *ACS nano*, 2014, **8**, 6312–6320.

45 S. Kim, Y. T. Lim, E. G. Soltesz, A. M. De Grand, J. Lee, A. Nakayama, J. A. Parker, T. Mihaljevic, R. G. Laurence, D. M. Dor, L. H. Cohn, M. G. Bawendi and J. V. Frangioni, *Nature Biotechnology*, 2004, **22**, 93–97.

46 W. Cai, D.-W. Shin, K. Chen, O. Gheysens, Q. Cao, S. X. Wang, S. S. Gambhir and X. Chen, *Nano Letters*, 2006, **6**, 669–676.

47 J. P. Zimmer, S.-w. Kim, S. Ohnishi, E. Tanaka, J. V. Fran-

View Article Online
DOI: 10.1039/C8TB00153G

gioni and M. G. Bawendi, *Journal of the American Chemical Society*, 2006, **128**, 2526–2527.

48 P. Yu, M. C. Beard, R. J. Ellingson, S. Fernere, C. Curtis, J. Drexler, F. Luiszer and A. J. Nozik, *Journal of Physical Chemistry B*, 2005, **109**, 7084–7087.

49 J. Park, C. Dvoracek, K. H. Lee, J. F. Galloway, H. E. C. Bhang, M. G. Pomper and P. C. Searson, *Small*, 2011, **7**, 3148–3152.

50 A. Ustione and D. W. Piston, *Journal of Microscopy*, 2011, **243**, 221–226.

51 W. R. Zipfel, R. M. Williams and W. W. Webb, *Nature biotechnology*, 2003, **21**, 1369–1377.

52 D. R. Larson, W. R. Zipfel, R. M. Williams, S. W. Clark, M. P. Bruchez, F. W. Wise and W. W. Webb, *Science (New York, N.Y.)*, 2003, **300**, 1434–1436.

53 Q. Liu, B. Guo, Z. Rao, B. Zhang and J. R. Gong, *Nano Letters*, 2013, **13**, 2436–2441.

54 L. M. Maestro, E. M. Rodríguez, F. S. Rodríguez, M. C. I.-d. la Cruz, A. Juarranz, R. Naccache, F. Vetrone, D. Jaque, J. a. Capobianco and J. G. Solé, *Nano letters*, 2010, **10**, 5109–5115.

55 H. Meng, J. Y. Chen, L. Mi, P. N. Wang, M. Y. Ge, Y. Yue and N. Dai, *Journal of Biological Inorganic Chemistry*, 2011, **16**, 117–123.

56 U. Bazylińska, S. Drozdek, M. Nyk, J. Kulbacka, M. Samoć and K. A. Wilk, *Langmuir*, 2014, **30**, 14931–14943.

57 K.-T. Yong, G. Xu and I. Roy, *Chemical communications (Cambridge, England)*, 2011, **47**, 2901–2903.

58 D. J. Bharali, D. W. Lucey, H. Jayakumar, H. E. Pudavar and P. N. Prasad, *Journal of the American Chemical Society*, 2005, **127**, 11364–11371.

59 M. Geszke, M. Murias, L. Balan, G. Medjahdi, J. Korczynski, M. Moritz, J. Lulek and R. Schneider, *Acta Biomaterialia*, 2011, **7**, 1327–1338.

60 L. Wang and R. K. Jain, *Journal of the Optical Society of America B*, 2009, **26**, 2161–2166.

61 H. Hafian, A. Sukhanova, M. Turini, P. Chames, D. Baty, M. Pluot, J. H. M. Cohen, I. Nabiev and J. M. Millot, *Nanomedicine*, 2014, **10**, 1701–1709.

62 A. Sukhanova, H. Hafian, M. Turini, P. Chames, D. Baty, M. Pluot, J. H. M. Cohen, J. M. Millot and I. Nabiev, *Materials Today: Proceedings*, 2016, **3**, 523–526.

63 L. M. Maestro, C. Jacinto, U. Rocha, M. Carmen Igleslasde Ia Cruz, F. Sanz-Rodrlguez, A. Juarranz, J. G. Solé and D. Jaque, *Journal of Applied Physics*, 2012, **111**, 023513.

64 K.-T. Yong, I. Roy, R. Hu, H. Ding, H. Cai, J. Zhu, X. Zhang, E. J. Bergey and P. N. Prasad, *Integrative biology*, 2010, **2**, 121–129.

65 M. Geszke-Moritz, H. Piotrowska, M. Murias, L. Balan, M. Moritz, J. Lulek and R. Schneider, *Journal of Materials Chemistry B*, 2013, **1**, 698–706.

66 S. A. Blanton, A. Dehestani, P. C. Lin and P. Guyot-Sionnest, *Chemical Physics Letters*, 1994, **229**, 317–322.

67 D. Pan, J. Zhang, Z. Li and M. Wu, *Advanced Materials*, 2010, **22**, 734–738.

68 S. Kundu, R. M. Yadav, M. V. Shelke, N. T. Narayanan, R. Vajtai, P. M. Ajayan and V. K. Pillai, *Nanoscale*, 2015, **7**, 11515 – 11519.

69 C. M. Luk, M. K. Tsang, C. F. Chan and S. P. Lau, *International Scholarly and Scientific Research & Innovation*, 2014, **8**, 1387–1390.

70 J. Shen, Y. Zhu, C. Chen, X. Yang and C. Li, *Chemical Communications*, 2011, **47**, 2580–2582.

71 M. Li, W. Wu, W. Ren, H. M. Cheng, N. Tang, W. Zhong and Y. Du, *Applied Physics Letters*, 2012, **101**, 103107.

72 W.-S. Kuo, C.-Y. Chang, H.-H. Chen, C.-L. Hsu, J.-Y. Wang, H.-F. Kao, L.-S. Chou, Y.-C. Chen, S.-J. Chen, W.-T. Chang, S.-W. Tseng, P.-C. Wu and Y.-C. Pu, *ACS Applied Materials and Interfaces*, 2016, **8**, 30467–30474.

73 X. Feng, Z. Li, X. Li and Y. Liu, *Scientific Reports*, 2016, **6**, 33260.

74 D. Ren, Y. Xia, B. Wang and Z. You, *Analytical Chemistry*, 2016, **88**, 4318–4327.

75 Q. Xu, Y. Zhang, B. Tang and C. Y. Zhang, *Analytical Chemistry*, 2016, **88**, 2051–2058.

76 X. Qiu and N. Hildebrandt, *ACS Nano*, 2015, **9**, 8449–8457.

77 E. Petryayeva, W. R. Algar and I. L. Medintz, *Applied spectroscopy*, 2013, **67**, 215–252.

78 G. Rousserie, A. Sukhanova, K. Even-Desrumeaux, F. Fleury, P. Chames, D. Baty, V. Oleinikov, M. Pluot, J. H. M. Cohen and I. Nabiev, *Critical Reviews in Oncology/Hematology*, 2010, **74**, 1–15.

79 N. Hildebrandt and D. Geißler, *Nano-Biotechnology for Biomedical and Diagnostic Research*, 2012, vol. 733, pp. 75–86.

80 S. N. Baker and G. A. Baker, *Angewandte Chemie International Edition*, 2010, **49**, 6726–6744.

81 X. Wang, L. Cao, S. T. Yang, F. Lu, M. J. Meziani, L. Tian, K. W. Sun, M. A. Bloodgood and Y. P. Sun, *Angewandte Chemie International Edition*, 2010, **49**, 5310–5314.

82 S. Zhu, J. Zhang, C. Qiao, S. Tang, Y. Li, W. Yuan, B. Li, L. Tian, F. Liu, R. Hu, H. Gao, H. Wei, H. Zhang, H. Sun and B. Yang, *Chemical communications*, 2011, **47**, 6858–6860.

83 Z. Sheng Qian, X. Yue Shan, L. Jing Chai, J. Rong Chen and H. Feng, *Nanotechnology*, 2014, **25**, 415501.

84 A. Orte, J. M. Alvarez-Pez and M. J. Ruedas-Rama, *ACS Nano*, 2013, **7**, 6387–6395.

85 Y. Tao and D. T. Auguste, *Biosensors and Bioelectronics*, 2016, **81**, 431–437.

86 F. Shi, Y. Zhang, W. Na, X. Zhang, Y. Li and X. Su, *Journal of Materials Chemistry B*, 2016, **4**, 3278–3285.

87 R. Liu, D. Wu, X. Feng and K. Müllen, *Journal of the American Chemical Society*, 2011, **133**, 15221–15223.

88 J. Peng, W. Gao, B. K. Gupta, Z. Liu, R. Romero-aburto, L. Ge, L. Song, L. B. Alemany, X. Zhan, G. Gao, S. A. Vithayathil, B. A. Kaipparettu, A. A. Marti, T. Hayashi, J.-j. Zhu and P. M. Ajayan, *Nano Letters*, 2011, **12**, 844–849.

89 M. Nurunnabi, Z. Khatun, K. M. Huh, S. Y. Park, D. Y. Lee,

View Article Online
DOI: 10.1039/C8TB00153G

K. J. Cho and Y.-k. Lee, *ACS Nano*, 2013, **7**, 6858–6867.

90 A. Chandra, S. Deshpande, D. B. Shinde, V. K. Pillai and N. Singh, *ACS Macro Letters*, 2014, **3**, 1064–1068.

91 M. Nurunnabi, Z. Khatun, M. Nafiujjaman, D. G. Lee and Y.-k. Lee, *ACS Applied Materials and Interfaces*, 2013, **5**, 8246–8253.

92 C. K. Chua, Z. Sofer, P. Šimek, O. Jankovský, K. Klímová, S. Bakardjieva, Å. Hrdličková Kučková and M. Pumera, *ACS Nano*, 2015, **9**, 2548–2555.

93 J. Qiu, R. Zhang, J. Li, Y. Sang, W. Tang, P. R. Gil and H. Liu, *International Journal of Nanomedicine*, 2015, **10**, 6709–6724.

94 P. Nigam, S. Waghmode, M. Louis, S. Wangnoo, P. Chavan and D. Sarkar, *Journal of Materials Chemistry B*, 2014, **2**, 3190–3195.

95 Y. Chong, Y. Ma, H. Shen, X. Tu, X. Zhou, J. Xu, J. Dai, S. Fan and Z. Zhang, *Biomaterials*, 2014, **35**, 5041–5048.

96 Y. Sun, S. Wang, C. Li, P. Luo, L. Tao, Y. Wei and G. Shi, *Physical Chemistry Chemical Physics*, 2013, **15**, 9907–9913.

97 C. Wu, C. Wang, T. Han, X. Zhou, S. Guo and J. Zhang, *Advanced Healthcare Materials*, 2013, **2**, 1613–1619.

98 L. Zhou, J. Geng and B. Liu, *Particle & Particle Systems Characterization*, 2013, **30**, 1086–1092.

99 S. Zhu, N. Zhou, Z. Hao, S. Maharjan, X. Zhao, Y. Song, B. Sun, K. Zhang, J. Zhang, H. Sun, L. Lu and B. Yang, *RSC Advances*, 2015, **5**, 39399–39403.

100 Y. Qin, Z.-W. Zhou, S.-T. Pan, Z.-X. He, X. Zhang, J.-X. Qiu, W. Duan, T. Yang and S.-F. Zhou, *Toxicology*, 2015, **327**, 62–76.

101 Y. Dong, C. Chen, X. Zheng, L. Gao, Z. Cui, H. Yang, C. Guo, Y. Chi and C. M. Li, *Journal of Materials Chemistry*, 2012, **22**, 8764–8766.

102 F. L. Yuan, L. Ding, Y. C. Li, X. H. Li, L. Z. Fan, S. X. Zhou, D. C. Fang and S. H. Yang, *Nanoscale*, 2015, **7**, 11727–11733.

103 Y. Dong, J. Shao, C. Chen, H. Li, R. Wang, Y. Chi, X. Lin and G. Chen, *Carbon*, 2012, **50**, 4738–4743.

104 L. L. Li, J. Ji, R. Fei, C. Z. Wang, Q. Lu, J. R. Zhang, L. P. Jiang and J. J. Zhu, *Advanced Functional Materials*, 2012, **22**, 2971–2979.

105 Y. Li, Y. Hu, Y. Zhao, G. Shi, L. Deng, Y. Hou and L. Qu, *Advanced Materials*, 2011, **23**, 776–780.

106 A. Ananthanarayanan, X. Wang, P. Routh, B. Sana, S. Lim, D. H. Kim, K. H. Lim, J. Li and P. Chen, *Advanced Functional Materials*, 2014, **24**, 3021–3026.

107 Y. Li, Y. Zhao, H. Cheng, Y. Hu, G. Shi, L. Dai and L. Qu, *Journal of the American Chemical Society*, 2012, **134**, 15–18.

108 J. Ju and W. Chen, *Biosensors and Bioelectronics*, 2014, **58**, 219–225.

109 J. R. Lakowicz, *Principles of Fluorescence Spectroscopy*, Springer US, 3rd edn, 2006, ch. 1, pp. 1–27.

110 L. Damalakiene, V. Karabanovas, S. Bagdonas and R. Rotomskis, *International Journal of Molecular Sciences*, 2016, **17**, 473.

111 H. C. Ishikawa-Ankerhold, R. Ankerhold and G. P. C. Drummen, *Molecules*, 2012, **17**, 4047–4132.

112 A. Rück, C. Hülshoff, I. Kinzler, W. Becker and R. Steiner, *Microscopy research and technique*, 2007, **70**, 485–492.

113 H. Schneckenburger, M. Wagner, P. Weber, W. S. L. Strauss and R. Sailer, *Journal of Fluorescence*, 2004, **14**, 649–654.

114 S. Coda, A. J. Thompson, G. T. Kennedy, K. L. Roche, L. Ayaru, D. S. Bansi, G. W. Stamp, A. V. Thillainayagam, P. M. W. French and C. Dunsby, *Biomedical optics express*, 2014, **5**, 515–38.

115 H. E. Grecco, K. A. Lidke, R. Heintzmann, D. S. Lidke, C. Spagnuolo, O. E. Martinez, E. A. Jares-Erijman and T. M. Jovin, *Microscopy Research and Technique*, 2004, **65**, 169–179.

116 J. Conroy, S. J. Byrne, Y. K. Gun'ko, Y. P. Rakovich, J. F. Donegan, A. Davies, D. Kelleher and Y. Volkov, *Small*, 2008, **4**, 2006–2015.

117 J. J. Peterson and T. D. Krauss, *Physical Chemistry Chemical Physics*, 2006, **8**, 3851–3856.

118 E. Arnspang Christensen, P. Kulatunga and B. C. Lagerholm, *PLoS ONE*, 2012, **7**, e44355.

119 W. G. J. H. M. van Sark, P. L. T. M. Frederix, D. J. Van den Heuvel, H. C. Gerritsen, A. A. Bol, J. N. J. van Lingen, C. de Mello Donegá and A. Meijerink, *Journal of Physical Chemistry B*, 2001, **105**, 8281–8284.

120 X. T. Zheng, H. L. He and C. M. Li, *RSC Advances*, 2013, **3**, 24853–24857.

121 M. Ulusoy, J. Walter, A. Lavrentieva, I. Kretschmer, L. Sandiford, A. Le Marois, R. Bongartz, P. Aliuos, K. Suhling, F. Stahl, M. Green and T. Scheper, *RSC Advances*, 2015, **5**, 7485–7494.

122 H. Asami, Y. Abe, T. Ohtsu, I. Kamiya and M. Hara, *The Journal of Physical Chemistry B*, 2003, **107**, 12566–12568.

123 J. Kimura, T. Uematsu, S. Maenosono and Y. Yamaguchi, *Journal of Physical Chemistry B*, 2004, **108**, 13258–13264.

124 W. G. J. H. M. van Sark, P. L. T. M. Frederix, A. A. Bol, H. C. Gerritsen and A. Meijerink, *ChemPhysChem*, 2002, **3**, 871–879.

125 S. R. Cordero, P. J. Carson, R. A. Estabrook, G. F. Strouse and S. K. Buratto, *Journal of Physical Chemistry B*, 2000, **104**, 12137–12142.

126 B. C. Hess, I. G. Okhrimenko, R. C. Davis, B. C. Stevens, Q. A. Schulzke, K. C. Wright, C. D. Bass, C. D. Evans and S. L. Summers, *Physical Review Letters*, 2001, **86**, 3132–3135.

127 D. Gerion, F. Pinaud, S. C. Williams, W. J. Parak, D. Zanchet, S. Weiss and P. A. Alivisatos, *Journal of Physical Chemistry B*, 2001, **105**, 8861–8871.

128 L. Jing, S. V. Kershaw, Y. Li, X. Huang, Y. Li, A. L. Rogach and M. Gao, *Chemical Reviews*, 2016, **116**, 10623–10730.

129 H. Weller, U. Koch, M. Gutiérrez and A. Henglein, *Berichte der Bunsengesellschaft für Physikalische Chemie*, 1984, **88**, 649–656.

130 R. Rossetti, R. Hull, J. M. Gibson and L. E. Brus, *The Journal of Chemical Physics*, 1985, **82**, 552.

View Article Online
DOI: 10.1039/C8TB00153G

131 A. J. Nozik, F. Williams, M. T. Nenadović, T. Rajh and O. I. Mićić, *Journal of Physical Chemistry*, 1985, **89**, 397–399.
132 H. Weller, A. Fojtik and A. Henglein, *Chemical Physics Letters*, 1985, **117**, 485–488.
133 A. Fojtik, H. Weller and A. Henglein, *Chemical Physics Letters*, 1985, **120**, 552–554.
134 U. Resch, H. Weller and A. Henglein, *Langmuir*, 1989, **5**, 1015–1020.
135 A. Y. Rakovich, V. Stockhausen, A. S. Susha, S. Sapra and A. L. Rogach, *Colloids and Surfaces A: Physicochemical and Engineering Aspects*, 2008, **317**, 737–741.
136 P. Wu, T. Zhao, Y. Tian, L. Wu and X. Hou, *Chemistry*, 2013, **19**, 7473–7479.
137 N. Goswami, A. Giri, S. Kar, M. S. Bootharaju, R. John, P. L. Xavier, T. Pradeep and S. K. Pal, *Small*, 2012, **8**, 3175–3184.
138 Q. Wang, F. Ye, T. Fang, W. Niu, P. Liu, X. Min and X. Li, *Journal of Colloid and Interface Science*, 2011, **355**, 9–14.
139 N. Ma, T. Grigory and S. O. Kelley, *Accounts of Chemical Research*, 2010, **43**, 173–180.
140 S. Mussa Farkhani and A. Valizadeh, *IET nanobiotechnology*, 2014, **8**, 59–76.
141 C. M. Tyrakowski and P. T. Snee, *Physical Chemistry Chemical Physics*, 2014, **16**, 837–855.
142 C. B. Murray, D. Norris and M. G. Bawendi, *Journal of the American Chemical Society*, 1993, **115**, 8706–8715.
143 R. Rossetti and L. Brus, *The Journal of Physical Chemistry*, 1982, **86**, 4470–4472.
144 M. A. Hines and P. Guyot-Sionnest, *The Journal of Physical Chemistry*, 1996, **100**, 468–471.
145 B. O. Dabbousi, J. Rodriguez, F. V. Mikulec, J. R. Heine, H. Mattoussi, R. Ober, K. F. Jensen and M. G. Bawendi, *Journal of Physical Chemistry B*, 1997, **101**, 9463–9475.
146 I. L. Medintz, H. Mattoussi and A. R. Clapp, *International journal of nanomedicine*, 2008, **3**, 151–167.
147 J. Aldana, Y. A. Wang and X. Peng, *Journal of the American Chemical Society*, 2001, **123**, 8844–8850.
148 D. Liu and P. T. Snee, *ACS Nano*, 2011, **5**, 546–550.
149 A. M. Smith, H. Duan, M. N. Rhyner, G. Ruan and S. Nie, *Physical Chemistry Chemical Physics*, 2006, **8**, 3895–3903.
150 Z. M. Markovic, B. Z. Ristic, K. M. Arsikin, D. G. Klisic, L. M. Harhaji-Trajkovic, B. M. Todorovic-Markovic, D. P. Kepic, T. K. Kravic-Stevovic, S. P. Jovanovic, M. M. Milenkovic, D. D. Milivojevic, V. Z. Bumbasirevic, M. D. Dramicanin and V. S. Trajkovic, *Biomaterials*, 2012, **33**, 7084–7092.
151 X. Yan, X. Cui and L.-s. Li, *Journal of the American Chemical Society*, 2010, **132**, 5944–5945.
152 J. Xi, C. Xie, Y. Zhang, L. Wang, J. Xiao, X. Duan, J. Ren, F. Xiao and S. Wang, *ACS Applied Materials and Interfaces*, 2016, **8**, 22563–22573.
153 Q. Li, B. Chen and B. Xing, *Environmental Science & Technology*, 2017, **3**, 1364–1376.
154 X. Wang, X. Sun, H. He, H. Yang, J. Lao, Y. Song, Y. Xia, H. Xu, X. Zhang and F. Huang, *Journal of Materials Chemistry B*, 2015, **3**, 3583–3590.
155 T. Wang, S. Zhu and X. Jiang, *Toxicology Research*, 2015, **4**, 885–894.
156 X. Wang, X. Sun, J. Lao, H. He, T. Cheng, M. Wang, S. Wang and F. Huang, *Colloids and Surfaces B: Biointerfaces*, 2014, **122**, 638–644.
157 C.-L. Huang, C.-C. Huang, F.-D. Mai, C.-L. Yen, S.-H. Tzing, H.-T. Hsieh, Y.-C. Ling and J.-Y. Chang, *Journal of Materials Chemistry B*, 2015, **3**, 651–664.
158 V. A. Gérard, C. M. Maguire, D. Bazou and Y. K. Gun'ko, *Journal of Nanobiotechnology*, 2011, **9**, 50.
159 P. Suriamoorthy, X. Zhang, G. Hao, A. G. Joly, S. Singh, M. Hossu, X. Sun and W. Chen, *Cancer Nanotechnology*, 2010, **1**, 19–28.
160 M. Daela, H. Singh, U. Soni and S. Sapra, *Proceedings of the International Conference on Advanced Nanomaterials & Emerging Engineering Technologies*, 2013, 144–147.
161 Y.-Y. Ma, H. Ding and H.-M. Xiong, *Nanotechnology*, 2015, **26**, 305702.
162 R. Bilan, F. Fleury, I. Nabiev and A. Sukhanova, *Bioconjugate Chemistry*, 2015, **26**, 609–624.
163 A. Sukhanova, K. Even-Desrumeaux, P. Chames, D. Baty, M. Artemyev, V. Oleinikov and I. Nabiev, *Protocol Exchange*, 2012, DOI 10.1038/protex.2012.042.
164 T. Y. Rakovich, O. K. Mahfoud, B. M. Mohamed, A. Prina-Mello, K. Crosbie-Staunton, T. V. D. Broeck, L. D. Kimpe, A. Sukhanova, D. Baty, A. Rakovich, S. A. Maier, F. Alves, F. Nauwelaers, I. Nabiev, P. Chames and Y. Volkov, *ACS Nano*, 2014, **8**, 5682–5695.
165 A. Sukhanova, K. Even-Desrumeaux, A. Kisserli, T. Tabary, B. Reveil, J. M. Millot, P. Chames, D. Baty, M. Artemyev, V. Oleinikov, M. Pluot, J. H. M. Cohen and I. Nabiev, *Nanomedicine: Nanotechnology, Biology, and Medicine*, 2012, **8**, 516–525.
166 M. B. Zaman, T. N. Baral, Z. J. Jakubek, J. Zhang, X. Wu, E. Lai, D. Whitfield and K. Yu, *Journal of Nanoscience and Nanotechnology*, 2011, **11**, 3757–3763.
167 E. R. Goldman, E. D. Balighian, H. Mattoussi, M. K. Kuno, J. M. Mauro, P. T. Tran and G. P. Andersont, *Journal of the American Chemical Society*, 2002, **124**, 6378–6382.
168 J. Zhao, X. Qiu, Z. Wang, J. Pan, J. Chen and J. Han, *OncoTargets and Therapy*, 2013, **6**, 303–309.
169 R. Gui, A. Wan, Y. Zhang, H. Li and T. Zhao, *Analytical Chemistry*, 2014, **86**, 5211–5214.
170 Q. Yuan, S. Hein and R. D. K. Misra, *Acta Biomaterialia*, 2010, **6**, 2732–2739.
171 C. Wang, C. Wu, X. Zhou, T. Han, X. Xin, J. Wu, J. Zhang and S. Guo, *Scientific Reports*, 2013, **3**, 2852.
172 S. Some, A.-R. Gwon, E. Hwang, G.-h. Bahn, Y. Yoon, Y. Kim, S.-H. Kim, S. Bak, J. Yang, D.-G. Jo and H. Lee, *Scientific reports*, 2014, **4**, 6314.
173 H. I. Pass, *Journal of the National Cancer Institute*, 1993, **85**, 443–456.
174 T. J. Dougherty, C. J. Gomer, B. W. Henderson, G. Jori, D. Kessel, M. Korbelik, J. Moan and Q. Peng, *Journal of the*

View Article Online
DOI: 10.1039/C8TB00153G

National Cancer Institute, 1998, **90**, 889–905.

175 C. Hopper, *The Lancet Oncology*, 2000, **1**, 212–219.

176 S. B. Brown, E. A. Brown and I. Walker, *The Lancet Oncology*, 2004, **5**, 497–508.

177 D. W. Felsher, *Nature Reviews Cancer*, 2003, **3**, 375–379.

178 M. Ochsner, *Journal of Photochemistry and Photobiology B*, 1997, **39**, 1–18.

179 Á. Juarranz, P. Jaén, F. Sanz-Rodríguez, J. Cuevas and S. González, *Clinical and Translational Oncology*, 2008, **10**, 148–154.

180 J. Fuchs and J. Thiele, *Free Radical Biology and Medicine*, 1998, **24**, 835–847.

181 M. C. DeRosa and R. J. Crutchley, *Coordination Chemistry Reviews*, 2002, **233-234**, 351–371.

182 R. Bakalova, H. Ohba, Z. Zhelev, M. Ishikawa and Y. Baba, *Nature biotechnology*, 2004, **22**, 1360–1361.

183 A. C. S. Samia, X. Chen and C. Burda, *Journal of the American Chemical Society*, 2003, **125**, 15736–15737.

184 V. Morosini, T. Bastogne, C. Frochot, R. Schneider, A. François, F. Guillemin and M. Barberi-Heyob, *Photochemical & photobiological sciences*, 2011, **10**, 842–851.

185 A. C. S. Samia, S. Dayal and C. Burda, *Photochemistry and photobiology*, 2006, **82**, 617–625.

186 J. M. Tsay, M. Trzoss, L. Shi, X. Kong, M. Selke, M. E. Jung and S. Weiss, 2007, **129**, 6865–6871.

187 M. Nafiujjaman, M. Nurunnabi, S.-h. Kang, G. R. Reeck, H. A. Khan and Y.-k. Lee, *J. Mater. Chem. B*, 2015, **3**, 5815–5823.

188 K. Habiba, J. Encarnacion-Rosado, K. Garcia-Pabon, J. C. Villalobos-Santos, V. I. Makarov, J. A. Avalos, B. R. Weiner and G. Morell, *International Journal of Nanomedicine*, 2015, **11**, 107–119.

189 F. Wo, R. Xu, Y. Shao, Z. Zhang, M. Chu, D. Shi and S. Liu, *Theranostics*, 2016, **6**, 485–500.

190 K. Albert and H.-Y. Hsu, *Molecules*, 2016, **21**, 1585.

191 L. Zhou, L. Zhou, X. Ge, J. Zhou, S. Wei and J. Shen, *Chemical Communications*, 2014, **51**, 421–424.

192 S. P. Jovanović, Z. Syrgiannis, Z. M. Marković, A. Bonasera, D. P. Kepić, M. D. Budimir, D. D. Milivojević, V. D. Spasojević, M. D. Dramićanin, V. B. Pavlović and B. M. Todorović Marković, *ACS Applied Materials & Interfaces*, 2015, **7**, 25865–25874.

193 M. Nurunnabi, Z. Khatun, G. R. Reeck, D. Y. Lee and Y.-k. Lee, *ACS Applied Materials and Interfaces*, 2014, **6**, 12413–12421.

194 J. Ge, M. Lan, B. Zhou, W. Liu, L. Guo, H. Wang, Q. Jia, G. Niu, X. Huang, H. Zhou, X. Meng, P. Wang, C.-S. Lee, W. Zhang and X. Han, *Nature Communications*, 2014, **5**, 4596.

195 Y. Li, Z. Wu, D. Du, H. Dong, D. Shi and Y. Li, *RSC Advances*, 2016, **6**, 6516–6522.

196 X. Hu and X. Gao, *ACS Nano*, 2010, **4**, 6080–6086.

197 J. A. J. Fitzpatrick, S. K. Andreko, L. A. Ernst, A. S. Waggoner, B. Ballou and M. P. Bruchez, *Nano Letters*, 2009, **9**, 2736–2741.

198 H. Soo Choi, W. Liu, P. Misra, E. Tanaka, J. P. Zimmer, B. Itty Ipe, M. G. Bawendi and J. V. Frangioni, *Nature Biotechnology*, 2007, **25**, 1165–1170.

199 R. Weissleder, A. Bogdanov, E. A. Neuwelt and M. Papisov, *Advanced Drug Delivery Reviews*, 1995, **16**, 321–334.

200 A. M. Derfus, W. C. W. Chan and S. N. Bhatia, *Nano Letters*, 2004, **4**, 11–18.

201 W. C. W. Chan and S. Nie, *Science*, 1998, **281**, 2016–2018.

202 T. Pellegrino, L. Manna, S. Kudera, T. Liedl, D. Koktysh, A. L. Rogach, S. Keller, J. Rädler, G. Natile and W. J. Parak, *Nano Letters*, 2004, **4**, 703–707.

203 B. Dubertret, P. Skourides, D. J. Norris, V. Noireaux, A. H. Brivanlou and A. Libchaber, *Science*, 2002, **298**, 1759–1762.

204 X. Gao, Y. Cui, R. M. Levenson, L. W. K. Chung and S. Nie, *Nature Biotechnology*, 2004, **22**, 969–976.

205 S. T. Selvan, T. T. Tan and J. Y. Ying, *Advanced Materials*, 2005, **17**, 1620–1625.

206 M. Darbandi, R. Thomann and T. Nann, *Chemistry of Materials*, 2005, **17**, 5720–5725.

207 M. Bruchez Jr., M. Moronne, P. Gin, S. Weiss and A. P. Alivisatos, *Science*, 1998, **281**, 2013–2016.

208 R. Koole, M. M. van Schooneveld, J. Hilhorst, C. de Mello Donegá, D. C. 't Hart, A. van Blaaderen, D. Vanmaekelbergh and A. Meijerink, *Chemistry of Materials*, 2008, **20**, 2503–2512.

209 T. Zhang, J. L. Stilwell, D. Gerion, L. Ding, O. Elboudwarej, P. A. Cooke, J. W. Gray, A. P. Alivisatos and F. F. Chen, *Nano Letters*, 2006, **6**, 800–808.

210 R. Guo, S. Zhou, Y. Li, X. Li, L. Fan and N. H. Voelcker, *ACS Applied Materials and Interfaces*, 2015, **7**, 23958–23966.

211 N. Narayanaswamy and T. Govindaraju, *Sensors and Actuators B*, 2012, **161**, 304–310.

212 S. Wang, X. Meng and M. Zhu, *Tetrahedron Letters*, 2011, **52**, 2840–2843.

213 T. Pons, E. Pic, N. Lequeux, E. Cassette, L. Bezdetnaya, F. Guillemin, F. Marchal and B. Dubertret, *ACS Nano*, 2010, **4**, 2531–2538.

214 S. J. Byrne, Y. Williams, A. Davies, S. A. Corr, A. Rakovich, Y. K. Gun'ko, Y. P. Rakovich, J. F. Donegan and Y. Volkov, *Small*, 2007, **3**, 1152–1156.

215 B. I. Ipe, M. Lehnig and C. M. Niemeyer, *Small*, 2005, **1**, 706–709.

216 P. Juzenas, R. Generalov, A. Juzeniene and J. Moan, *Journal of Biomedical Nanotechnology*, 2008, **4**, 450–456.

217 M. Green and E. Howman, *Chemical Communications*, 2005, **0**, 121–123.

218 A. Anas, H. Akita, H. Harashima, T. Itoh, M. Ishikawa and V. Biju, *The Journal of Physical Chemistry B*, 2008, **112**, 10005–10011.

219 P. Juzenas, W. Chen, Y.-P. Sun, M. A. N. Coelho, R. Generalov, N. Generalova and I. L. Christensen, *Advanced Drug Delivery Reviews*, 2008, **60**, 1600–1614.

220 A. Rakovich, D. Savateeva, T. Rakovich, J. F. Donegan, Y. P.

View Article Online
DOI: 10.1039/C8TB00153G

Rakovich, V. Kelly, V. Lesnyak and A. Eychmüller, *Nanoscale Research Letters*, 2010, **5**, 753–760.

221 A. Rakovich, T. Rakovich, V. Kelly, V. Lesnyak, A. Eychmüller, Y. P. Rakovich and J. Donegan, *Journal of Nanoscience and Nanotechnology*, 2010, **10**, 2656–2662.

222 M. Kakran, N. G. Sahoo, H. Bao, Y. Pan and L. Li, *Current medicinal chemistry*, 2011, **18**, 4503–4512.

223 X. Wang, L. Cao, F. Lu, M. J. Meziani, H. Li, G. Qi, B. Zhou, B. A. Harruff, F. Kermarrec and Y.-P. Sun, *Chemical Communications*, 2009, **0**, 3774–3776.

224 I. L. Christensen, Y.-P. Sun and P. Juzenas, *Journal of Biomedical Nanotechnology*, 2011, **7**, 667–676.

225 B. Fadeel, A. Åhlin, J. I. Henter, S. Orrenius and M. B. Hampton, *Blood*, 1998, **92**, 4808–4818.

226 H.-U. Simon, A. Haj-Yehia and F. Levi-Schaffer, *Apoptosis*, 2000, **5**, 415–418.

227 S. T. Stern, B. S. Zolnik, C. B. McLeland, J. Clogston, J. Zheng and S. E. McNeil, *Toxicological Sciences*, 2008, **106**, 140–152.

228 N. Mizushima, B. Levine, A. M. Cuervo and D. J. Klionsky, *Nature*, 2008, **451**, 1069–1075.

229 T. S. Hauck, R. E. Anderson, H. C. Fischer, S. Newbigging and W. C. W. Chan, *Small*, 2010, **6**, 138–144.

230 H. C. Fischer, L. Liu, K. S. Pang and W. C. W. Chan, *Advanced Functional Materials*, 2006, **16**, 1299–1305.

231 A. Nagy, A. Steinbrück, J. Gao, N. Doggett, J. A. Hollingsworth and R. Iyer, *ACS Nano*, 2012, **6**, 4748–4762.

232 J.-H. Liu, S.-T. Yang, H. Wang, Y. Chang, A. Cao and Y. Liu, *Nanomedicine*, 2012, **7**, 1801–1812.

233 M. C. Duch, G. R. S. Budinger, Y. T. Liang, S. Soberanes, D. Urich, S. E. Chiarella, L. A. Campochiaro, A. Gonzalez, N. S. Chandel, M. C. Hersam and G. M. Mutlu, *Nano Letters*, 2011, **11**, 5201–5207.

234 S. Wang, I. S. Cole and Q. Li, *RSC Advances*, 2016, **6**, 89867–89878.

235 M. Jennifer and W. Maciej, *Journal of Biomaterials and Nanobiotechnology*, 2013, **04**, 53–63.

236 Y. Liu, L.-P. Xu, W. Dai, H. Dong, Y. Wen and X. Zhang, *Nanoscale*, 2015, **7**, 19060–19065.

237 R. A. Goyer, *Annual Review of Nutrition*, 1997, **17**, 37–50.

238 A. M. Jastrzębska, P. Kurtycz and A. R. Olszyna, *Journal of Nanoparticle Research*, 2012, **14**, 1320.

239 H. Key, E. R. Davies, P. C. Jackson and P. N. T. Wells, *Physics in Medicine and Biology*, 1991, **36**, 579–590.

240 M. Roy, C. J. Niu, Y. Chen, P. Z. McVeigh, A. J. Shuhendler, M. K. Leung, A. Mariampillai, R. S. Dacosta and B. C. Wilson, *Small*, 2012, **8**, 1780–1792.